Modeling ultrafine particle growth at a pine forest site influenced by anthropogenic pollution during BEACHON-RoMBAS 2011

Yuyan Cui[1], Alma Hodzic[2,*], James N. Smith[2,3], John Ortega[2], Jerome Brioude[4,5], Hitoshi Matsui[6], Ezra J. T. Levin[7], Andrew Turnipseed[2], Paul Winkler [2,8], Benjamin de Foy[1]

[1] Department of Earth and Atmospheric Sciences, Saint Louis University, MO

[2] National Center for Atmospheric Research, Atmospheric Chemistry Division, P.O. Box 3000, Boulder, CO 80307.

[3] Department of Applied Physics, University of Eastern Finland, FIN-70211, Kuopio, Finland.

[4] Chemical Sciences Division, Earth System Research Laboratory, NOAA, Boulder, Colorado, 80305.

[5] Cooperative Institute for Research in Environmental Sciences, University of Colorado, Boulder, CO 80309.

[6] Japan Agency for Marine-Earth Science and Technology, Kanagawa, Japan.

[7] Department of Atmospheric Science, Colorado State University, Fort Collins, Colorado, USA.

[8] Faculty of Physics, University of Vienna, Boltzmanngasse 5, 1090 Vienna, Austria.

*Corresponding author: Alma Hodzic (alma@ucar.edu)

Abstract

Formation and growth of ultrafine particles is crudely represented in chemistry-climate models, contributing to uncertainties in aerosol composition, size distribution, and aerosol effects on cloud condensation nuclei (CCN) concentrations. Measurements of ultrafine particles, their precursor gases, and meteorological parameters were performed in a ponderosa pine forest in the Colorado Front Range in July–August 2011, and were analyzed to study processes leading to small Particle Burst Events (PBEs) which were characterized by an increase in the number concentrations of ultrafine 4-30 nm diameter size particles. These measurements suggest that PBEs were associated with the arrival at the site of anthropogenic pollution plumes mid-day to early afternoon. During PBEs, number concentrations of 4-30 nm diameter particles typically exceeded 10^4 cm^{-3}, and these elevated concentrations coincided with increased SO_2 and monoterpene concentrations, and led to a factor-of-two increase in CCN concentrations at

0.5% supersaturation. The PBEs were simulated using the regional WRF-Chem model, which was extended to account for ultrafine particle sizes starting at 1 nm in diameter, to include an empirical activation nucleation scheme in the planetary boundary layer, and to explicitly simulate the subsequent growth of Aitken particles (10-100 nm) by condensation of organic and inorganic vapors. The updated model reasonably captured measured aerosol number concentrations and size distribution during PBEs, as well as ground level CCN concentrations. Model results suggest that sulfuric acid originating from anthropogenic SO_2 triggered PBEs, and that the condensation of monoterpene oxidation products onto freshly nucleated particles contributes to their growth. The simulated growth rate of ~3.4 nm hr^{-1} for 4-40 nm diameter particles was comparable to the measured average value of 2.3 nm hr^{-1}. Results also suggest that the presence of PBEs tends to modify the composition of sub-20 nm diameter particles, leading to a higher mass fraction of sulfate aerosols. Sensitivity simulations suggest that the representation of nucleation processes in the model largely influences the predicted number concentrations and thus CCN concentrations. We estimate that nucleation contributes to 67% of surface CCN at 0.5% supersaturation in this pine forest environment.

1. Introduction

Submicron particles reduce atmospheric visibility, impact human health, and influence climate by radiative forcing and by modifying the number of cloud condensation nuclei (CCN) (Somers et al., 2004; Laaksonen et al., 2005). To accurately predict these effects, precise estimates of the aerosol size distribution are required (Adams and Seinfeld, 2002; Dusek et al., 2010) in addition to the typically-reported mass concentrations. Modeling aerosol size distributions is challenging due to uncertainties involved in the formation and growth of new particles (Pierce et al., 2011). A new particle formation event is the result of complex processes where molecular clusters (1 – 2 nm) are created by nucleation of gases that can subsequently

grow into detectable-sized particles depending on the outcome of two competing processes: condensation of semi-volatile organic and inorganic gases and coagulation to preexisting particles (Kulmala et al., 2003; Kerminen and Kulmala, 2002; McMurry et al., 2005). Studies have shown that nucleated clusters originate from sulfuric acid, water, ammonia, and organic compounds (Zhang et al., 2004; Sipilä et al., 2010; Kulmala et al., 2013, Kirkby et al., 2011), however the mechanisms of formation are still being developed. Ultrafine aerosols can become active CCN with changes in their size distribution and chemical properties and thus can have an impact on cloud properties, precipitation and regional climate (McFiggans et al., 2006, Rosenfeld et al., 2008). Kerminen et al. (2005) estimated that cloud droplets originated from new particle formation over the boreal forests in Finland are associated with a radiative cooling of 0.2-0.9 Wm^{-2}.

Predicting nucleation events and their effect on CCN concentrations is challenging and the results largely depend on the selected nucleation scheme and the environmental conditions. Previous studies have reported that binary and ternary homogeneous nucleation schemes (nucleation of H_2SO_4) that are commonly used in 3D climate models tend to underestimate nucleation rates and particle number concentrations by orders of magnitude, especially within the boundary layer (e.g. Kulmala et al., 2006; Young et al., 2008). Merikanto et al. (2009) used activation nucleation (AN) parameterization (Kulmala et al., 2006) in the boundary layer and binary homogeneous nucleation in the free troposphere, and estimated that nucleation contributes to 45% of global mean CCN (0.2% Super Saturation (SS)), of which 35% can be attributed to the flux of nucleated particles from the free troposphere and 10% from the boundary layer. Matsui et al. (2011) used a similar approach within a regional model in the polluted urban environment of Beijing, and predicted that new particle formation increased CCN concentrations at high (>0.2%) supersaturations, and decreased CCN at low (<0.1%)

supersaturation. Given the uncertainties in available parameterizations, Pierce et al. (2009) compared several nucleation schemes that spanned six orders of magnitude in globally averaged nucleation rates, and estimated that the average tropospheric CCN concentrations varied by less than 17% in the troposphere, and by 12% within the boundary layer at low (0.2%) supersaturations. Although the global CCN predictions were only moderately sensitive to the choice of nucleation scheme, the presence of nucleation was found to be crucial for predicting CCN. Luo and Yu (2011) used the ion-mediated nucleation scheme and predicted that new particle formation accounted for 80% of CCN (0.4% SS) in most parts of the Eastern United States.

Aerosol nucleation and subsequent growth have been observed in various environments including urban areas (Matsui et al., 2011), coastal regions (O'Dowd et al., 2002), rural and forest environments (Kulmala et al., 2001; Levin et al., 2012; Pierce et al., 2012). In the current study, we define the term "small Particle Burst Event" (PBE) to describe the appearance and growth of particles that are larger than 3 nm in diameter in contrast with typical nucleation events that include particles between 1 and 3 nm. Here PBEs refer to both nucleation-mode particles (< 10nm) and Aitken-mode particles (10-100nm). Particle formation events, whether arising from local nucleation of new particles or PBE-type events, have frequently been observed in clean forest air masses, for example in Finland (Kulmala et al., 2001). However it is unclear if the same types of processes are occurring in forests influenced by anthropogenic pollution because urban plumes contain gases that both contribute to the onset of nucleation and also contain sufficient concentrations of pre-existing particles on to which condensable gases can partition instead of nucleating. Understanding how forest environments respond to the inflow of pollutants from the nearby cities is of great scientific interest as populations at the forest-urban interfaces are increasing. Jung et al. (2013) showed that the inflow of urban air

masses could favor the initiation of the burst of nucleation mode particles in an isoprene-rich deciduous forest in Northern Japan. However, studies in other types of forests, such as terpene-rich forests, are less conclusive. As part of the Bio-hydro-atmosphere interactions of Energy, Aerosols, Carbon, H_2O, Organics & Nitrogen (BEACHON, Ortega et al., 2014) project long-term measurements of trace gases, aerosols and meteorological parameters at the Manitou Experimental Forest Observatory (MEFO). This site is located within a semi-arid ponderosa pine forest in the Colorado Front Range. It is representative of an urban-rural interface and provides a unique opportunity to study aerosol formation in a monoterpene-rich environment that is periodically influenced by the inflow of anthropogenic pollution from Denver and Colorado Springs (DiGangi et al., 2012; Fry et al., 2013; Ortega et al., 2014). The PBEs events observed at the site during the summer months were found to coincide with an increase in CCN concentrations at high supersaturations (Levin et al., 2012), but the origin of the ultrafine particle formation events was not investigated.

In this paper, we use data from the BEACHON Rocky Mountain Biogenic Aerosol Study (RoMBAS) intensive measurement period (July 25 to August 25, 2011) to investigate the origin of ultrafine aerosol formation and growth events, and to model their characteristics using the regional Weather Research and Forecasting model with chemistry (WRF-Chem, Grell et al., 2005, Fast et al., 2006). More specifically, we will use measurements and model simulations to (1) characterize the connection between anthropogenic pollution and the occurrence of PBEs, (2) to test the ability of the WRF-Chem model to predict the levels of ultrafine particles during PBE episodes at the site, and (3) to quantify their influences on CCN concentrations. As biogenic emissions dominate the volatile organic compound concentrations at this site (Kaser et al., 2013, Ortega et al., 2014), their effects on the growth of newly nucleated particles will

also be investigated. The WRF-Chem model is particularly well suited for this study as it simultaneously treats biogenic emissions, chemistry and CCNs.

2. Measurement site and circulation patterns during the campaign

The Manitou Experimental Forest Observatory (MEFO; 39.1006° N, 105.0942° W) is located in the Front Range of the Colorado Rockies at ~2,300 m elevation in a subalpine forest dominated by ponderosa pine (Fig. 1). It is located 40 km northwest of Colorado Springs and 72 km southwest of Denver. The site is frequently influenced by polluted air from the Front Range urban areas. Previous studies at MEFO have indicated that monoterpenes and 2-methyl-3-butene-2-ol (MBO) are the dominant component of VOC emissions during the daytime (Kim et al., 2010; Kaser et al., 2013; Ortega et al., 2014). Concentrations of anthropogenic pollutants (e.g NO_x, SO_2, benzene) observed at the site are variable and driven by synoptic and local meteorological conditions. Meteorological observations from the meteorological tower at MEFO have been used to analyze the diurnal variations of wind speeds and wind directions during both the BEACHON-ROCS (2010) and BEACHON-RoMBAS (2011) campaigns (Ortega et al., 2014). During daytime in the summer, easterly upslope flows are often observed at MEFO with wind speeds of 2-3 m s^{-1}, whereas during nighttime strong southwesterly drainage flows dominate with typical wind speeds around 3-5 m s^{-1}. PBE's at MEFO almost always occur during mid-day, and it is suspected that these events are related to transport from the urban areas to the east.

3. Measurements and modeling framework

3.1 Datasets

Measurements from several instruments are used in this study to characterize PBEs during BEACHON-RoMBAS 2011. Particle size distributions from 4 nm to 3 μm were measured on a

5-minute cycle. The method consists of two Scanning Mobility Particle Sizers (SMPS) that measure particles from 4 nm to 30 nm and from 30 nm to 300 nm, and an optical particle counter that measures particles from 200 nm to 3 μm. The final data set is composed of the superposition of the 3 different measurements. The chemical composition of 20 nm diameter aerosol performed during BEACHON-RoMBAS was obtained by the Thermal Desorption Chemical Ionization Mass Spectrometer (TDCIMS, Voisin et al., 2003; Smith et al., 2004). During non-PBE periods and during weak events, the TDCIMS measured the composition of bulk aerosol (< 1 μm), whereas during PBEs (such as August 10) the instrument measured the composition of 20 nm diameter particles. The TDCIMS acquired data in "negative ion mode" using the reagent ion O_2-(H_2O)n, where n is in the range of 1-3, which allows for the detection of inorganic and organic acids. Proton Transfer Reaction Quadrupole Mass Spectrometers (PTR-MS) measured ambient monoterpenes and MBO – the dominant emissions from ponderosa pine. We also use gas-phase measurements of CO, NO_x, SO_2 and H_2SO_4 meteorological measurements of wind speeds and direction (at 30 m height), and measurements of CCN concentrations. The latter measurements were mostly performed at 0.5% SS with critical activation diameters less than 65 nm, and included the corresponding derived hygroscopicity parameter, kappa, for sub-100 nm particles (Petters and Kreidenweis, 2007). Size-resolved CCN measurements were made with a differential mobility analyzer (DMA; TSI 3071) followed by a Droplet Measurement Technologies-Cloud condensation nuclei counter (DMT-CCNC) and a condensation particle counter (CPC; TSI 3010) (Levin et al., 2012, 2014). In this paper, the time is presented in Mountain Standard Time (MST).

We also calculate the condensation sink (CS, in s^{-1}, Eqn. 1), which is the rate that condensable inorganic and organic vapors condense onto pre-existing aerosols.

$$CS = 2\pi D_i \sum_j d_j \beta_m(K_{n_j}, \alpha) N_j \qquad (1)$$

where D_i is the gas-phase diffusion coefficient of condensable gas *i* (m^2 s^{-1}), N_j is the number concentrations (m^{-3}) of particle *j* with diameter d_j (m), β_m is the transitional correction for the condensational mass flux, and is a function of the Knudsen number K_{nj} ($= 2\lambda/d_j$) and the mass accommodation coefficient α, given by Fuchs & Sutugin (1971), with λ=6.8x10^{-8} m and α =0.1 in this study. The formation rate (J; see eqn. 2 below) and the growth rate are estimated from available measurements, starting at 4.4 nm diameter, and are used to constrain the WRF-Chem model. To determine the formation rate of ~5nm particles (J_{5nm}), we linearly fit the measured number concentrations of particles over the range of 4.4-6.25 nm diameter between the onset and the end of PBEs. The slope of the fitted line provides the measured formation rate (J_{5nm}) that is used to evaluate the model calculated formation rate for the model bin 3.98-6.31 nm. A similar method is applied to derive the formation rates for particles between 39-65 nm (J_{50nm}) and 101-162 nm (J_{130nm}) in the measurements, and their model equivalent values based on model bin 40-63 nm and bin 100-158 nm, respectively. It should be noted that the formation rate calculated here is the net formation rate which includes loss rates. We use the number mean diameter (NMD) to calculate the growth rate of particles in both measurements and simulations. NMD was defined by Matsui et al. (2011) using the diameter (nm) and number concentration (cm^{-3}) in each size bin. We use a linear fit to the values of NMD for particles smaller than 30 nm during PBEs, and the slope of the fitted line is defined as the sub-30 nm growth rate. Additionally, we calculate the hygroscopicity parameter, κ, by including all aerosol species present in the model for particles smaller than 100nm (see section 4.4).

3.2 WRF-Chem simulations

Version 3.4.1 of the Weather Research and Forecasting model with chemistry (WRF-Chem, Grell et al., 2005, Fast et al., 2006) was used with two nested domains over the continental

United States. The grid resolution was 36 km for domain 1 and 4 km for domain 2 (Fig 1). Two-way nesting was used between the domains. The WRF physics options chosen for our runs include the Monin–Obukhov scheme for the surface layer, the Yonsei University (YSU) scheme (Hong et al., 2006) for the planetary boundary layer, the Grell 3D scheme (Grell and Devenyi, 2002) for the cumulus parameterization in the 36km domain, the Lin et al. scheme for microphysics (Lin et al., 1983), the Rapid Radiative Transfer Model (Mlawer et al., 1997) for longwave radiation, and the Goddard scheme (Chou et al., 1998) for shortwave radiation. The nighttime minimum planetary boundary layer (PBL) height was set to 100 m in the YSU scheme based on previous studies (Choi et al., 2011) to eliminate overestimating nocturnal concentrations of primary species. The land cover treatment was updated with MODIS land use data. North American Regional Reanalysis (NARR) data was used for the initial and boundary conditions at a 3-hour temporal resolution and 32 km spatial resolution. Two representative periods were selected for our study: July 25-30 and August 09-15. The first 24 hours of each run were used to initialize the model, but were not used for comparisons. The meteorological outputs (such as wind field, PBL height, etc.) from WRF-Chem were used to drive a Lagrangian particle dispersion off-line model (see section 3.3) to estimate the arrival of anthropogenic plumes at the MEFO site.

The chemistry is simulated using the CBMz gas-phase mechanism (Zaveri et al., 1999) and MOSAIC aerosol package (Zaveri et al., 2008). Similar to Matsui et al. (2011), we have modified the MOSAIC aerosol package in WRF-Chem v3.4.1 to explicitly account for a wider range of aerosol sizes, i.e., 20 bins over the aerosol diameter range from 1 nm to 10 μm. The default 8 bins over the range are from 40 nm to 10 μm. The default binary homogenous nucleation scheme (Wexler et al., 1994) is used above the PBL, and it has been replaced by the

empirical AN scheme within the PBL. The number concentration of nucleated clusters based on the empirical AN scheme is given by Kulmala et al. (2006):

$$J^* = A \times [H_2SO_4] \quad (2)$$

where J* is the formation rate of activated clusters at 1 nm (cm^{-3} s^{-1}), A (s^{-1}) is the rate coefficient, and [H_2SO_4] is the number concentration of gas-phase sulfuric acid (cm^{-3}). Previous studies indicate a large uncertainty associated with calculations of A, which was found to range between 10^{-5} s^{-1} and 10^{-8} s^{-1} (Kuang et al., 2008). Here we estimate a representative value of A at our site based on measured H_2SO_4 and number concentrations of ultrafine particles. The H_2SO_4 measurements are available from 9 to 26 August at MEFO and indicate that the average H_2SO_4 concentration is ~ 2 x 10^6 molecules cm^{-3} during the late morning and early afternoon. During the campaign, the smallest particles with diameters of ~5nm were detected at the site on July 28, and their number concentrations were used to determine the 5 nm aerosol formation rate (J_{5nm}= ~ 1 cm^{-3} s^{-1} as shown in Table 1). The rate coefficient A of 2 x 10^{-6} s^{-1} was derived from those measurements, and is used within WRF-Chem for the AN parameterization to introduce particles into the first model size bin (1-4nm). We assume here that J_{5nm} is a representative value (the lower bound) of formation rate in the model first bin, which is a reasonable assumption at high H_2SO_4 concentrations typically observed during PBE days (Kulmala et al., 2006). The derived value of A is consistent with previous studies. E.g. Sihto et al. (2006) reported A=1.7 x 10^{-6} s^{-1}, whereas Matsui et al. (2011) used the value of 2 x 10^{-7} s^{-1} which was a factor of 10 lower in order to compensate for a 10-fold overprediction of H_2SO_4 concentrations in WRF-Chem.

In addition, sulfuric acid concentrations could not be estimated for this study (Mikkonen et al., 2011; Petäjä et al., 2009) as OH measurements were not available during the considered time

period. We attempted to more accurately simulate ultrafine particles growth by including the condensation of semi-volatile oxidation products of isoprene, α-pinene and limonene onto pre-existing particles. The default WRF-Chem model configuration only includes primary organic aerosols (Matsui et al., 2011), and accounting for the formation of secondary organic aerosols from biogenic precursors is important due to their abundance at this location. Simple molar yield calculations were used to estimate secondary organic aerosols formation, assuming 15% contribution for α-pinene and limonene, and 4% for both isoprene (Liu et al., 2012) and MBO (Zhang et al., 2014). To reduce the computational costs, the condensed mass was distributed in proportion to the aerosol surface area in each size bin. This simplification is consistent with other studies (e. g. Spracklen et al., 2006, Reddington et al., 2011) and assumes that the first generation oxidation products condense onto pre-existing particles with zero equilibrium vapor pressure.

Initial and boundary conditions for chemical species were provided by the MOZART-4 global chemistry-transport model (Emmons et al., 2010). For emissions, the EPA National Emission Inventory 2005 was used for the anthropogenic sources. The number size distribution of primary aerosol emissions was assumed to be a lognormal distribution with a median diameter of 50 nm and a standard deviation (a sigma) of 2. The MEGAN on-line model was applied for biogenic emissions (Guenther et al., 2006). Wet scavenging and dry deposition of gases and aerosols were also considered. The aerosol direct and indirect effects on radiation and cloud microphysics were included according to Gustafson et al. (2007) and Chapman et al. (2009).

Table 2 summarizes the WRF-Chem simulations and their characteristics. The base run (Ref-8bins) is the original WRF-Chem model with eight diameter bins starting at 40 nm. It includes the binary homogeneous nucleation parameterization in all vertical layers and does not account

for the formation of secondary organic compounds (similar to Fast et al., 2009). The first test run (Nucleation-on) uses 20 bins and simulates the number concentration with the AN parameterization in the PBL and binary homogeneous nucleation parameterization above the PBL. The second test run (Nucleation-bsoa) is similar to Nucleation-on run but in addition it includes the condensation of biogenic oxygenated semi-volatile organic compounds and their contribution to the growth of ultrafine particles. A final sensitivity run (Nucleation-off) uses 20 bins and includes the condensation of biogenic oxygenated semi-volatile organic compounds, but does not include a nucleation parameterization (neither AN nor binary).

3.3 The trajectory model

To investigate the transport of anthropogenic air masses to the MEFO site during the field study period, the Lagrangian particle dispersion model FLEXPART is used with WRF (WRF-FLEXPART, Stohl et al., 2005; Fast et al., 2006; Brioude et al., 2013). The wind field used to drive FLEXPART was a time-averaged wind predicted by the WRF-Chem 4 km simulations. We used the time-averaged wind to systematically decrease the uncertainty and bias in the trajectory calculations (Brioude et al., 2012). In WRF-FLEXPART, the vertical diffusion coefficients were calculated based on the mixing heights and surface friction velocity from WRF-Chem. At the MEFO site, 10,000 inert tracer particles are released every hour at a random height between 50 and 100m above the ground. For each release, the backward trajectories are simulated for 48 hours. The total calculation time is 30 days from July 27 to August 25, 2013, and the number of releases is 720. The hourly particle positions from the back trajectories are gridded onto the 4 x 4 km^2 WRF-Chem domain to perform the Residence Time Analysis. These gridded trajectories indicate the time that air masses spent in each grid cell before arriving at MEFO (de Foy et al., 2007, 2008), which illustrates the preferred wind directions and wind transport paths influencing the measurement site.

4. Results and discussion

4.1 Characterization of PBE and Non-PBE days

The temporal evolution of aerosol number size distributions observed during the entire campaign is shown in Fig. 2a. To distinguish between PBE and Non-PBE days, we calculate the ratio of the number concentrations of 4-30 nm particles ($N_{4\text{-}30nm}$) to the concentrations of 4-100 nm particles ($N_{4\text{-}100nm}$). When the ratio was larger than 0.5 (Jung et al., 2013) and the diurnal evolution of the aerosol number size distribution was characterized by a banana-shaped plot (Dal Maso et al., 2005), we classified that event as a PBE day. Using these criteria, we selected four representative PBEs (July 28, 29 and August 10, 13, see Fig. 2b), and three representative Non-PBEs days (August 14, 23, and 24). Fig. 2b shows the observed temporal evolution of SO_2 mixing ratios and $N_{4\text{-}30nm}$ at MEFO during the campaign. $N_{4\text{-}30nm}$ was correlated with SO_2 (Pearson correlation coefficient is 0.8), with $N_{4\text{-}30nm}$ peak values that systematically coincided with high SO_2 observed at the site. These results suggest that the inflow of anthropogenic pollutants impacts PBEs at the MEFO site, and that the PBEs are likely initiated by SO_2 oxidation products. The daily cycle of monoterpenes (Fig. 2b) exhibits a more consistent day-to-day cycle with higher values at night, and lower values at the midday. Isoprene concentrations were low at the site (Ortega et al., 2014) and are not shown here. A closer look at the diurnal evolution of the number size distribution during the PBE event of July 28 (Figs 3a,b) shows the typical banana-shaped growth of the number size distributions. The sharp increase in both $N_{4\text{-}30nm}$ and $N_{30\text{-}100nm}$ particles coincides with the shift in wind directions from westerly to northeasterly (from the Denver metropolitan area).

Observations of averaged diurnal profiles of SO_2, CO, monoterpenes, $N_{4\text{-}30nm}$, CCN (0.5% SS), and number size distribution confirm the existence of large differences between PBE and Non-PBE days (Fig. 4). Significantly higher mean values are observed during PBE days for both

monoterpenes and SO_2, and it is clear that $N_{4\text{-}30nm}$ is dramatically starting midday during PBE days (Fig 4c). CO levels are also higher during PBE days, which confirm that the MEFO site is influenced by the inflow of anthropogenic pollutants. Primary particles transported from the Front Range are not expected to significantly contribute to $N_{4\text{-}30nm}$ concentrations because anthropogenic emissions typically generate larger particles (e.g. 30-40 nm, Brines et al., 2014). To appreciate how rapidly molecules condense onto pre-existing aerosols, we also compare the condensation sink (CS) between PBE and Non-PBE days. CS values range from $3x10^{-3}$ to $7x10^{-3}$ s^{-1} (Fig. 4e), and are typical of forest areas (Dal Maso et al., 2002). Somewhat higher (~ 1.5 times) CS values are found on PBE days just before the onset of PBEs (Figs. 4e and S2), which indicates higher concentrations of pre-existing particles on those days before the start of PBEs. During PBE days, the CS values decrease to their minimum around midday, which is generally the PBE onset time, and then progressively increase due to the growth of the ultrafine particles to larger sizes. There is also a large difference in size distributions between PBE and Non-PBE days for particles smaller than 150 nm (Fig 4f), which is typically the size range that encompasses the critical activation diameters for CCN (50-100nm) (Petters and Kreidenweis, 2007). The peak of the number size distribution is shifted from ~110 nm on Non-PBE days to smaller diameters ~30 nm on PBE days. Measured CCN (0.5% SS) number concentrations at the surface are also up to a factor of two higher during afternoon hours on PBE days compared to Non-PBE days (Fig 3f). A sharp increase in CCN is observed in the afternoon, typically three hours after the start of PBEs. It should be noted that only particles larger than ~60nm are likely to activate at 0.5% SS (Dusek et al., 2006). Given the observed growth rates of 2.3 nm hr^{-1} (Table 1), it would take >20 hours for freshly nucleated particles to reach a diameter of 60nm. Therefore, the higher CCN concentrations on PBE days are likely the result of the enhanced growth of pre-existing particles. Finally, the comparison of measured ambient 2m temperatures (Fig. S1, first panel) shows 1-2 degrees cooler temperatures during PBE days.

Table 1 shows the observed and predicted formation and growth rates for ~5 nm, ~50 nm, and ~130 nm diameter particles, and number concentrations of 4-40 nm ($N_{4\text{-}40nm}$) and 40-100 nm ($N_{40\text{-}100nm}$) particles for PBEs that occurred at MEFO on July 28 and 29, and August 10. The PBEs at the MEFO site typically started around noon and early afternoon (10:20–15:00 MST, Table 1) following a shift in wind directions generally to the east (Fig 5a). This late onset time was reported for other forest sites (Jung et al., 2013). $N_{4\text{-}40nm}$ and $N_{40\text{-}100nm}$ reported in Table 1 are calculated as average values over a two-hour time period following the peak of each PBE. Here, we report particles from 4 to 40 nm instead of 4 to 30 nm in order to have a closer match with the corresponding bins in the simulations. The observed $N_{4\text{-}40nm}$ averaged during the event, varies from ~16,000 to ~28,000 cm^{-3}, and $N_{40\text{-}100nm}$ from ~4,000 to 12,000 cm^{-3}. $N_{4\text{-}40nm}$ is three to four times higher compared to $N_{40\text{-}100nm}$. The observed number size distribution during these PBE days (Fig S4) shows a relatively broad distribution similar to previous studies performed in an anthropogenically-influenced forest (Jung et al., 2013). Fig. S4 also shows the absence of particles smaller than 5nm. Especially in August (Fig. 8a), particles smaller than 10 nm were almost never observed suggesting that nucleation likely occurred in upwind areas or in the free troposphere, and that freshly nucleated particles grew for several hours before reaching the measurement site. It should be noted that the PBE episode of August 13 was very atypical showing an inverse banana-shaped growth (Fig. 8a). The FLEXPART back-trajectories show that this "shrinkage" in the observed number size distribution could be related to the change in the air mass that is being sampled over the site during this event. The arrival of a polluted air mass from the Colorado Springs area during the afternoon (see Fig S5) is a likely reason for the appearance of smaller particles, which could have been nucleated slightly upwind of the measurement site.

For all PBEs, the average growth rate was estimated to be 2.3 nm hr^{-1}, and the average net rates of formation for ~5 nm, ~50 nm, and ~130 nm particles to 0.74 cm^{-3} s^{-1}, 0.18 cm^{-3} s^{-1}, and 0.013 cm^{-3} s^{-1}, respectively. The values derived from these observations are consistent with previous results reported for other forested regions (Kuang et al., 2008; Westervelt et al., 2013). The comparisons between observations and simulations are discussed in section 4.3.

4.2 Inflow of anthropogenic pollutants at MEFO

To investigate the relationship between PBEs and the transport of anthropogenic pollutants to the site, we have analyzed the origin of the air masses arriving at the measurement site prior to PBEs. The wind roses measured at MEFO at a 30 m height show the variation of wind direction by time of day for PBE and Non-PBE days (Figs. 5a,b). During PBE days, wind directions clearly show a shift from southwesterly in the early morning (6:00-9:00 MST) to easterly and then to southeasterly or northeasterly winds during the day (10:00-17:00 MST). The dominant easterly wind component indicates influence from the Front Range urban areas, whereas on non-PBE days, there are more consistently from the southwest. Because the measured near-surface winds at the site can be greatly influenced by local topography, we have performed the Residence Time Analysis based on the FLEXPART back-trajectories to confirm the origin of the air masses for the PBE and Non-PBE days. The right panels of Figs. 5a and b show that on PBE days air masses at MEFO came from the Colorado Springs area, whereas on Non-PBE days the air masses are principally from the west. The results suggest that elevated SO_2 likely originated from industrial sources located in the Colorado Springs area. Consistent with measurements (Fig. 3), back-trajectory results emphasize the key role of anthropogenic pollutants in the occurrence of ultrafine particle events at the MEFO site.

The average time for the air mass to be transported to MEFO during PBE days was estimated to ~4h for air masses originating in Colorado Springs, and to ~7h for air masses from the Denver metropolitan area. Given the estimated transport time, and the estimated growth rates of ~3nm hr^{-1}, particles arriving from Denver would have grown by ~20-30nm during transportation time to the site, whereas particles arriving from Colorado Springs would have grown by ~15nm. It should be noted that primary emitted particles in the model have sizes of 50nm, and would appear at the MEFO site as 70-80nm particles if they originated from Denver, and as ~65nm particles if they originated from Colorado Springs. Therefore their contribution to sub-40nm particles predicted at the site during PBE days is unlikely. Only particles that nucleated over urban areas and smaller than 10nm could contribute to the sub-40nm at MEFO if they were transported to the site. However, the nucleation events over urban areas are infrequent as the condensable gases preferably partition onto existing particles, which are typically abundant in urban areas.

4.3 Evaluation of modeled PBEs

The regional WRF-Chem model is used to simulate PBEs and analyze interactions between anthropogenic and biogenic air masses, as well as the potential influence of PBEs on CCN concentrations at the MEFO ground site. As mentioned in section 3.2, the model includes both the AN parameterization that connects the anthropogenic SO_2 emissions to nucleation, and the contributions of biogenic VOC emissions to the growth of ultrafine particles. Comparisons with measurements of O_3, CO and NO_2 (Fig S6) suggest that WRF-Chem generally captures their overall magnitudes and temporal variability during PBEs. Due to the complex mountain terrain, predicting the arrival of narrow pollution plumes at the site is challenging especially with the current model resolution of 4 km. For instance on July 29, WRF-Chem did not capture the observed SO_2 plume at the site because of a west shift bias in the simulated wind direction.

On August 10, simulated SO_2 was much lower than observations because of an excessively large westerly component in simulated winds. These biases in simulated SO_2 influence the predicted levels of H_2SO_4 and lead to model underestimation of PBEs on those days (e.g., $N_{4\text{-}40nm}$ Figs. 7 and 8).

Given the difficulty in predicting local meteorology, we examine (Fig. 6) the model's ability to reproduce the average features observed during PBE and Non-PBE days. For that purpose, average diurnal profiles of observed and predicted parameters associated with number size distributions of sub-100nm particles are examined. It is important to keep in mind that $N_{4\text{-}40nm}$ is controlled by regional scale nucleation and early particle growth, whereas $N_{40\text{-}100nm}$ is also influenced by regional transport and anthropogenic emissions. The comparison of the number concentrations shows a noticeable improvement in model predictions when the Nucleation-bsoa run is used compared to the default WRF-Chem configuration (Ref-8bins). The default configuration does not explicitly simulate $N_{4\text{-}40nm}$, and greatly underestimates (up to a factor of 4) the $N_{40\text{-}100nm}$ concentrations during both PBE and Non-PBE days. The Nucleation-bsoa run captures well the increase in $N_{4\text{-}40nm}$ during PBE days, although it has a tendency to nucleate some particles during Non-PBE days as suggested by somewhat overpredicted $N_{4\text{-}40nm}$ concentrations. This could be an artifact of the implementation of the AN parameterization in WRF-Chem which used measured formation rates of 5nm particles to introduce nucleated particles into the model first bin, and could lead to an overprediction of freshly nucleated particles at low H_2SO_4 concentrations as discussed in section 3.2. Simulation results (Fig 6e) are clearly improved in terms of number mean diameters (NMD). During PBEs, the increase in number concentrations of ultrafine particles ($N_{4\text{-}40nm}$) leads to a NMD reduction at midday (12-18 MST) to values as low as ~30nm, followed by an increase in NMD in the late afternoon due to the condensational growth. As expected the default Ref-8bins run did not capture the

decrease in NMD during the early afternoon, caused by the appearance of freshly nucleated particles on PBE days. Observations (Fig. 3g) show that the peak of the number size distribution is shifted from ~110nm on Non-PBE days to smaller diameters ~30nm on PBE days. This shift in NMDs was well predicted by the Nucleation-bsoa run (Fig. S7). The comparison of modeled (Nucleation-bsoa) number size distributions between PBE and Non-PBE days shows the same shift in the peak diameter from ~100nm on Non-PBE days to ~40nm on PBE days. During Non-PBE days, the Nucleation-bsoa run predicts slightly better the observed evolution of NMD than Ref-8bins (Fig. 6f).

A more detailed day-to-day evaluation of predicted number concentrations and size distributions for sub-100nm particles is shown for July 26-30 (Fig. 7), and August 10-14 (Fig. 8). As mentioned in section 4.1, during July PBEs had a more typical banana-shaped size distribution and particles down to 5nm were observed, suggesting that new-particle formation likely occurred close to the measurement site. During this period, the updated WRF-Chem (Nucleation-bsoa run) was able to reproduce the banana shape of the number size distributions (Figs. 7a and 7b). The time series comparisons show that the Nucleation-bsoa simulation roughly captures the variations in number concentrations of sub-40nm particles (Fig. 7c) and the diurnal evolution of the number mean diameter (NMD) (Fig. 7e). The model however has a tendency to overpredict the number concentrations of larger $N_{40\text{-}100nm}$ particles and does not capture the sharp increase in those on July 29. During August, PBEs were characterized by larger starting diameters (>10nm) suggesting that new particle formation occurred upwind of the site or above the PBL, and that already somewhat grown particles were transported to the site. During this period, the WRF-Chem, Nucleation-bsoa run, initiated some local nucleation but did not grow these particles beyond 4 nm on August 10, 11 and 14, and not beyond 8 nm on August 12 (Fig. 8b). Model results suggest that the sub-100 nm particles that were both

predicted and observed at the site on these days were not locally generated through nucleation. Sensitivity simulations were performed for the PBE day of August 10 to investigate the contribution of the transport of pre-existing particles and of the above-PBL nucleation to predicted sub-100nm particles (Fig. S8). In the first sensitivity simulation, the nucleation parameterization was turned off in the model, and the resulting simulation showed very low number concentrations of sub-100nm particles (<500 cm^{-3}, Fig. 8d). In the second simulation, the binary nucleation parameterization was used above the PBL and no nucleation was used within the PBL. The results suggest that the above-PBL nucleation explained 90% of the ultrafine particles predicted at the surface on this particular day (Fig. S8b). The results from combined Nucleation-bsoa and sensitivity runs suggest that locally formed new particles were not able to grow to detectable sizes, and that free-troposphere nucleated particles could have been mixed downward into the boundary layer and contributed to observed >10nm particles. On August 13, the model starts nucleating particles locally but does not grow them to larger sizes. Larger particles are however predicted later in the afternoon (after 5pm MST) and are likely due to changes in the air mass. Local wind roses and back-trajectories (Fig S5) both suggest a shift in wind direction from southwest to southeast during that afternoon, which advected polluted air from Colorado Springs to the measurement site as already discussed in section 4.1. This change in the air mass could have brought already nucleated ultrafine particles to the site. As illustrated in Fig. 8c (no-nucleation run), the contribution of primary emitted particles to simulated sub-40nm is expected to be negligible as these particles are emitted into the larger size bins (centered at 50 nm diameter).

Modeled 4-40 nm diameter growth rates, and formation rates (J_{5nm}, J_{50nm}, J_{130nm}) are shown in Table 1. In comparison with observations, we find that Nucleation-bsoa slightly overestimates the growth rates of sub-40nm. In addition, the formation rates are underestimated for 50nm

particles (J_{50nm}) and overestimated for 100nm particles (J_{130nm}) by the model. Predicted $N_{4\text{-}40nm}$ and $N_{40\text{-}100nm}$ values are comparable to observations, with the exception of $N_{4\text{-}40nm}$ on July 29 and August 10 which is underestimated even in the Nucleation-bsoa run. These results indicate that the model configuration and spatial resolutions are not sufficiently accurate to capture all of the nucleation sources, and perhaps that the physical and chemical conditions encountered during nucleation events are not adequately represented by measurements performed at MEFO.

4.4 Sensitivity to the treatment of nucleation

There are large differences in simulation results in time series due to changes in the nucleation representation in WRF-Chem (Figs. 7c-e and 8c-e). As already shown, the default WRF-Chem simulation (Ref-8bins) does not explicitly simulate sub-40nm particles, and shows large biases in $N_{40\text{-}100nm}$ concentrations (Figs. 7c,d, 8c,d) and NMD (Figs. 7e, 8e) during the campaign. The number size distributions are not captured during the PBE days suggesting that this default model version is not suitable for studying aerosol effect on CCN and clouds in forested environments. As expected, large differences with observations are found for the simulation that does not account for nucleation processes (nucleation-off) with a factor of 5 underprediction of both $N_{4\text{-}40nm}$ and $N_{40\text{-}100nm}$ levels. Results from runs that include nucleation without condensational growth by organic vapors (nucleation-on) generally overestimate $N_{4\text{-}40nm}$ and underpredicts the observed NMD by a factor of 2 suggesting that ultrafine particle growth is not captured by the model. The comparison between Nucleation-on and Nucleation-bsoa runs emphasizes the key role of biogenic VOC to the growth of freshly nucleated particles. The presence of biogenic secondary organic aerosol formation in the Nucleation-bsoa run results in a decrease of $N_{4\text{-}40nm}$, by almost an order of magnitude, and an increase in $N_{40\text{-}100nm}$ by a factor of 2 compared with Nucleation-on. Nucleation-bsoa better simulates $N_{40\text{-}100nm}$ during

PBE days but overestimates $N_{40\text{-}100nm}$ during Non-PBE days. Overall, our results suggest that the condensational growth from semi-volatile organic compounds plays an important role in PBEs over the Colorado Front Range, and that including the AN representation in the model considerably improves the simulation of PBEs.

4.5 Composition of ultrafine particles during PBEs and effects on CCN

TDCIMS measurements shown in Fig. 9a suggest that ultrafine aerosols observed at MEFO during PBE days are enriched in sulfate. The molar ratio of water-soluble species, which is defined as the abundance of a specific ion divided by the sum of all ion abundances, suggests that sub-20 nm particles during the PBE event of August 10 are made of ~61% sulfate, ~37% organics and <1% nitrate. These values are similar to aerosol mass spectrometer measurements of bulk submicron (< 1 μm) aerosol composition averaged for August 8, 9 and 11 during Non-PBE days. The plot shows a clear difference in the relative abundance of sulfate during the PBE (~61%) vs. Non-PBE events (~41%). However, this increase in sulfate cannot be attributed to the presence of PBEs, due to the difference in size distributions considered here (20nm vs. submicron).

Fig. 9b shows simulated mass fractions of sulfate and organics in ~20nm particles during PBEs days (Jul 28, 29, and August 10) and Non-PBEs days (August 11 and 14). Results for PBEs show a factor of two increases in the relative contribution of sulfate to aerosol mass concentrations relative to Non-PBE days. However, the relative fraction of sulfate in ~20 nm particles during PBEs is larger in the measurements than in model predictions. This difference could result from the limitations in the detection of organic species by the TDCIMS instrument leading to an underprediction of the relative fraction of organics compared to sulfate. The fact

that we are considering different days could also explain this discrepancy (i.e. measurements report values for August 10, whereas the model results are averaged over several PBE days). Model predictions for August 10 (Fig. S8) show a higher fraction of sulfate (~40%). In addition, model results for the Nucleation-bsoa simulation (Fig. S9) indicate that organic aerosols account for 40 to 75% of the ultrafine (4-20nm) particulate mass. The comparison with the Nucleation-off sensitivity simulation that has a factor of 3 lower amounts of sulfate, ammonium, and organics in the 4-20 nm range, illustrates the importance of nucleation processes in predicting the ultrafine aerosol composition (see Fig. S9).

Changes in submicron particle composition during PBEs can affect their hygroscopicity, and therefore modify their ability to form CCN. Here we compare the measured and predicted volume-averaged hygroscopicity parameter (kappa) (Fig. 10). For calculations of kappa in WRF-Chem, we consider typical hygroscopicity values shown in parentheses (Chapman et al., 2009) for individual compounds including sulfate (0.5), ammonium (0.5), nitrate (0.5), black carbon (10^{-6}), organic compounds (0.14), other inorganics (OIN, 0.14), sodium (1.16), chloride (1.16). The calculated kappa value is the average of the hygroscopicity of individual species weighted by their respective volume concentrations for aerosol sizes below 100 nm. For the Nucleation-bsoa run, the model reasonably simulates the measured values of kappa. The Nucleation-bsoa simulation generally captures kappa variability in the time series (Figs. 10a,b) except for the lowest observed values during the nighttime that are overestimated by the model. We should note that July 29 has very high values of kappa (>0.3) indicative of an increased contribution of sulfate aerosols during the PBE event. The model does not reproduce those high values, at least in part because the simulations do not capture the SO_2 transport adequately on this day (see section 4.3). The comparison of average diurnal profiles of observed and predicted kappa values during PBE and Non-PBE days (Figs. 6g-6h) shows that the

Nucleation-bsoa run improves simulations of hygroscopicity compared to the model default simulation Ref-8bins. In both the Nucleation-bsoa run and measurements, Kappa values vary from ~0.05 to 0.2 during PBE and Non-PBE days, and these values are typically a factor of two lower than the default model simulation (Ref-8bins) which doesn't account for the formation of secondary organic aerosols. Although Nucleation-bsoa simulates an increase in the afternoon values of Kappa that increase is not as pronounced as in the observations (Fig 6g).

The time series of measured and simulated CCN (0.5% SS) number concentrations are shown in Figs. 10c-d. In this study, CCN concentrations are calculated at 0.5% SS in the WRF-Chem model. As CCN measurements were mainly performed at high supersaturation (section 3.1), here we compare model results with CCN observations at 0.5% SS. As previously mentioned (sect 4.1), only particles with diameters larger than 60 nm are likely to activate at 0.5% SS. The Nucleation-bsoa run reasonably simulates the CCN (0.5% SS) concentrations in both time series (Fig. 10c,d) and diurnal profiles (Fig. 6i,j) except on 29 July as expected. Fig. 6i shows that the Nucleation-bsoa run captures the magnitudes of CCN (0.5% SS) during the daytime, with however a slight underestimation of the afternoon values during PBE days. The Nucleation-bsoa simulation reproduces more accurately CCN (0.5% SS) concentrations than the Ref-8bins run, especially during PBE days. This difference suggests that sub-40nm particles and their growth to larger sizes (>60nm) that can activate at 0.5% SS significantly contributes to CCN. The Nucleation-off simulation underestimates by a factor of 3 the CCN (0.5% SS) number concentration compared to Nucleation-bsoa (Fig 10). This indicates that the ability of the modified WRF-Chem to predict PBEs is dependent on including both AN nucleation parameterization and SOA formation. Comparing the results of Nucleation-bsoa with Nucleation-off during the two simulating periods, we find that the nucleation explains 67% of near-surface CCN (0.5% SS) concentrations at the MEFO site. This is an extreme case,

however it illustrates that the accurate treatment of nucleation in 3D models is important to predicting CCN (0.5% SS) concentrations and aerosol number concentration in general.

5. Summary and Conclusions

Small particle burst events (PBEs), indicative of nucleation-mode and Aitken-mode particles, were observed at the MEFO site during the 2011 BEACHON-RoMBAS field campaign. Four representative PBEs were studied that showed a rapid increase in the number of 4-30 nm diameter particles from midday to early afternoon in this region. Number concentrations of 4 to 40nm particles ranged from ~16,000 to 28,000 cm^{-3}, and 40 to 100nm particles ranged from 4,000 to 12,000 cm^{-3}. The average growth rate during PBEs of sub-40 nm particles was 2.3 nm hr^{-1}, and the average formation rates of ~5 nm, ~50 nm, and ~130 nm diameter particles during PBEs were 0.74 cm^{-3} s^{-1}, 0.18 cm^{-3} s^{-1}, and 0.013 cm^{-3} s^{-1} respectively. The size distributions of ultrafine particles imply that non-local nucleation sources, including air masses originating above the PBL and upwind sources, impact MEFO. The diurnal profiles of SO_2 and monoterpene concentrations were investigated during PBE and Non-PBE days. Considerable differences between PBEs and Non-PBEs indicate that pollution plumes rich in SO_2 combined with primary particles that were advected from the Colorado Front Range. Furthermore, enhanced biogenic monoterpenes concentrations significantly affect particle number concentrations and CCN during PBE days.

A modified version of the WRF-Chem model was applied to study PBEs during this campaign. The model was extended to include a parameterization of Activation Nucleation (AN) and the formation of SOA from biogenic and anthropogenic precursors. It also was used to simulate the corresponding volume-averaged hygroscopicity parameter (kappa) and CCN concentrations.

Comparisons with the default WRF-Chem model (containing 8 particle diameter bins and binary homogeneous nucleation parameterization) indicate that AN parameterization more accurately simulates PBEs in the 4-100nm size range, including onset times, number concentrations and number mean diameters. The sensitivity simulations using the updated model without nucleation parameterization suggest that PBEs influence the composition of small particles. Furthermore, the updated WRF-Chem simulations were able to represent variations and magnitudes of kappa and number concentration of CCN (0.5% SS), suggesting that the model can be used to study the connection between new particle formation and cloud formation. Our results from the enhanced WRF-Chem model highlighted the important role of the mixing of urban and forest air masses in the formation of PBEs, and the value of the MEFO site in studying PBEs due to its location at the intersection of different air masses, and with help of improved treatment of PBEs in CCN simulations and future research for other representative forest sites adjacent to urban areas.

Acknowledgements

The authors would like to acknowledge data contributions, interesting discussions and editing from Lisa Kaser (University of Innsbruck, Austria, and ASP postdoc at National Center for Atmospheric Research, NCAR), Ezra Levin (Colorado State University), David Gochis (National Center for Atmospheric Research, NCAR), Jerome Fast (Pacific Northwest National Laboratory, PNNL), and Christoph Knote (National Center for Atmospheric Research, NCAR). This research has been supported by the DOE DE-FG0208ER64627 grant, and NCAR which is operated by the University Corporation for Atmospheric Research on behalf of the National Science Foundation. Authors would like to thank in particular the generous support of the NCAR's Advanced Study Program / Graduate Visitor Program. PMW acknowledges financial support from the Austrian Science Fund (FWF, Project No. J3198-N21). JNS acknowledges

support from the National Science Foundation (ATM-0919317) and US Department of Energy (DE-SC0006861).

References

Adams, P. J. and Seinfeld, J. H.: Predicting global aerosol size distributions in general circulation models, J. Geophys. Res.-Atmos., 107, 2002.

Brioude, J., Angevine, W. M., McKeen, S. A., and Hsie, E. Y.: Nu- merical uncertainty at mesoscale in a Lagrangian model in complex terrain, Geosci. Model Dev., 5, 1127–1136, 2012.

Brioude, J., Arnold, D., Stohl, A., Cassiani, M., Morton, D., Seib- ert, P., Angevine, W., Evan, S., Dingwell, A., Fast, J. D., Easter, R. C., Pisso, I., Burkhart, J., and Wotawa, G.: The Lagrangian particle dispersion model FLEXPART-WRF version 3.1, Geosci. Model Dev., 6, 1889–1904, 2013.

Chapman, E. G., Gustafson, W. I., J., Easter, R. C., Barnard, J. C., Ghan, S. J., Pekour, M. S., and Fast, J. D.: Coupling aerosol- cloud-radiative processes in the WRF-Chem model: Investigating the radiative impact of elevated point sources, Atmos. Chem. Phys., 9, 945–964, 2009.

Choi, W., Faloona, I. C., McKay, M., Goldstein, A. H., and Baker, B.: Estimating the atmospheric boundary layer height over sloped, forested terrain from surface spectral analysis during BEARPEX, Atmos. Chem. Phys., 11, 6837–6853, 2011.

Chou, M. D., Suarez, M. J., Ho, C. H., Yan, M. M. H., and Lee, K. T.: Parameterizations for cloud overlapping and shortwave single-scattering properties for use in general circulation and cloud ensemble models, J. Climate, 11, 202–214, 1998.

Dal Maso, M., Kulmala, M., Lehtinen, K. E. J., Makela, J. M., Aalto, P., and O'Dowd, C. D.: Condensation and coagulation sinks and formation of nucleation mode particles in coastal and boreal forest boundary layers, J. Geophys. Res.-Atmos., 107, 2002.

Dal Maso, M., Kulmala, M., Riipinen, I., Wagner, R., Hussein, T., Aalto, P. P., and Lehtinen, K. E. J.: Formation and growth of fresh atmospheric aerosols: eight years of aerosol size distribution data from SMEAR II, Hyytiala, Finland, Boreal Environ. Res., 10, 323–336, 2005.

de Foy, B., Lei, W., Zavala, M., Volkamer, R., Samuelsson, J., Mel- lqvist, J., Galle, B., Martinez, A. P., Grutter, M., Retama, A., and Molina, L. T.: Modeling constraints on the emission inventory and on vertical dispersion for CO and SO_2 in the Mexico City Metropolitan Area using Solar FTIR and zenith sky UV spectroscopy, Atmos. Chem. Phys., 7, 781–801, 2007.

de Foy, B., Fast, J. D., Paech, S. J., Phillips, D., Walters, J. T., Coulter, R. L., Martin, T. J., Pekour, M. S., Shaw, W. J., Kasten- deuch, P. P., Marley, N. A., Retama, A., and Molina, L.

T.: Basin- scale wind transport during the MILAGRO field campaign and comparison to climatology using cluster analysis, Atmos. Chem. Phys., 8, 1209–1224, 2008.

DiGangi, J. P., Henry, S. B., Kammrath, A., Boyle, E. S., Kaser, L., Schnitzhofer, R., Graus, M., Turnipseed, A., Park, J. H., Weber, R. J., Hornbrook, R. S., Cantrell, C. A., Maudlin, R. L., Kim, S., Nakashima, Y., Wolfe, G. M., Kajii, Y., Apel, E. C., Goldstein, A. H., Guenther, A., Karl, T., Hansel, A., and Keutsch, F. N.: Observations of glyoxal and formaldehyde as metrics for the anthropogenic impact on rural photochemistry, Atmos. Chem. Phys., 12, 9529–9543, 2012.

Dusek, U., Frank, G. P., Curtius, J., Drewnick, F., Schneider, J., Kurten, A., Rose, D., Andreae, M. O., Borrmann, S., and Poschl, U.: Enhanced organic mass fraction and decreased hygroscopic- ity of cloud condensation nuclei (CCN) during new particle formation events, Geophys. Res. Lett., 37, 2010.

Emmons, L. K., Apel, E. C., Lamarque, J. F., Hess, P. G., Avery, M., Blake, D., Brune, W., Campos, T., Crawford, J., DeCarlo, P. F., Hall, S., Heikes, B., Holloway, J., Jimenez, J. L., Knapp, D. J., Kok, G., Mena-Carrasco, M., Olson, J., O'Sullivan, D., Sachse, G., Walega, J., Weibring, P., Weinheimer, A., and Wiedinmyer, C.: Impact of Mexico City emissions on regional air quality from MOZART-4 simulations, Atmos. Chem. Phys., 10, 6195–6212, 2010.

Fast, J. D., Gustafson, William I., J., Easter, R. C., Zaveri, R. A., Barnard, J. C., Chapman, E. G., Grell, G. A., and Peckham, S. E.: Evolution of ozone, particulates, and aerosol direct radiative forcing in the vicinity of Houston using a fully coupled meteorology-chemistry-aerosol model, J. Geophys. Res.-Atmos., 111, 2006.

Fast, J., Aiken, A. C., Allan, J., Alexander, L., Campos, T., Cana- garatna, M. R., Chapman, E., DeCarlo, P. F., de Foy, B., Gaffney, J., de Gouw, J., Doran, J. C., Emmons, L., Hodzic, A., Herndon, S. C., Huey, G., Jayne, J. T., Jimenez, J. L., Kleinman, L., Kuster, W., Marley, N., Russell, L., Ochoa, C., Onasch, T. B., Pekour, M., Song, C., Ulbrich, I. M., Warneke, C., Welsh-Bon, D., Wied- inmyer, C., Worsnop, D. R., Yu, X. Y., and Zaveri, R.: Evaluating simulated primary anthropogenic and biomass burning organic aerosols during MILAGRO: implications for assessing treatments of secondary organic aerosols, Atmos. Chem. Phys., 9, 6191–6215, 2009.

Fuchs, N., and A. Sutugin,: High-dispersed aerosols, in Topics in Current Aerosol Research, vol. 2, pp. 1–60, edited by G. M. Hidy and J. R. Brock, Pergamon, Oxford, U. K. 1971.

Fry, J. L., Draper, D. C., Zarzana, K. J., Campuzano-Jost, P., Day, D. A., Jimenez, J. L., Brown, S. S., Cohen, R. C., Kaser, L., Hansel, A., Cappellin, L., Karl, T., Roux, A. H., Turnipseed, A., Cantrell, C., Lefer, B. L., and Grossberg, N.: Observations of gas- and aerosol-phase organic nitrates at BEACHON-RoMBAS 2011, Atmos. Chem. Phys., 13, 8585–8605, 2013.

Grell, G. A. and Devenyi, D.: A generalized approach to parameterizing convection combining ensemble and data assimilation techniques, Geophys. Res. Lett., 29, 4, 2002.

Grell, G. A., Peckham, S. E., Schmitz, R., McKeen, S. A., Frost, G., Skamarock, W. C., and Eder, B.: Fully coupled "online" chemistry within the WRF model, Atmos. Environ., 39, 6957–6975, 2005.

Guenther, A., Karl, T., Harley, P., Wiedinmyer, C., Palmer, P. I., and Geron, C.: Estimates of global terrestrial isoprene emissions using MEGAN (Model of Emissions of Gases and

Aerosols from Nature), Atmos. Chem. Phys., 6, 3181–3210, 2006.

Gustafson, William I., J., Chapman, E. G., Ghan, S. J., Easter, R. C., and Fast, J. D.: Impact on modeled cloud characteristics due to simplified treatment of uniform cloud condensation nuclei during NEAQS 2004, Geophys. Res. Lett., 34, 2007.

Hong, S. Y., Noh, Y., and Dudhia, J.: A new vertical diffusion pack- age with an explicit treatment of entrainment processes, Mon. Weather Rev., 134, 2318–2341, 2006.

Jung, J., Miyazaki, Y., and Kawamura, K.: Different characteristics of new particle formation between urban and deciduous forest sites in Northern Japan during the summers of 2010-2011, Atmos. Chem. Phys., 13, 51–68, 2013.

Kaser, L., Karl, T., Schnitzhofer, R., Graus, M., Herdlinger-Blatt, I. S., DiGangi, J. P., Sive, B., Turnipseed, A., Hornbrook, R. S., Zheng, W., Flocke, F. M., Guenther, A., Keutsch, F. N., Apel, E., and Hansel, A.: Comparison of different real time VOC measurement techniques in a ponderosa pine forest, Atmos. Chem. Phys., 13, 2893–2906, 2013.

Kerminen, V. M. and Kulmala, M.: Analytical formulae connecting the ”real” and the ”apparent” nucleation rate and the nuclei number concentration for atmospheric nucleation events, J. Aerosol Sci., 33, 609–622, 2002.

Kerminen, V. M., Lihavainen, H., Komppula, M., Viisanen, Y., and Kulmala, M.: Direct observational evidence linking atmospheric aerosol formation and cloud droplet activation, Geophys. Res. Lett., 32, 2005.

Kim, S., Karl, T., Guenther, A., Tyndall, G., Orlando, J., Harley, P., Rasmussen, R., and Apel, E.: Emissions and ambient distributions of Biogenic Volatile Organic Compounds (BVOC) in a ponderosa pine ecosystem: interpretation of PTR-MS mass spectra, Atmos. Chem. Phys., 10, 1759–1771, 2010.

Kirkby, J., Curtius, J., Almeida, J., Dunne, E., Duplissy, J., Ehrhart, S., Franchin, A., Gagne, S., Ickes, L., Kurten, A., Kupc, A., Met- zger, A., Riccobono, F., Rondo, L., Schobesberger, S., Tsagkoge- orgas, G., Wimmer, D., Amorim, A., Bianchi, F., Breitenlechner, M., David, A., Dommen, J., Downard, A., Ehn, M., Flagan, R. C., Haider, S., Hansel, A., Hauser, D., Jud, W., Junninen, H., Kreissl, F., Kvashin, A., Laaksonen, A., Lehtipalo, K., Lima, J., Love- joy, E. R., Makhmutov, V., Mathot, S., Mikkila, J., Minginette, P., Mogo, S., Nieminen, T., Onnela, A., Pereira, P., Petaja, T., Schnitzhofer, R., Seinfeld, J. H., Sipila, M., Stozhkov, Y., Strat- mann, F., Tome, A., Vanhanen, J., Viisanen, Y., Vrtala, A., Wag- ner, P. E., Walther, H., Weingartner, E., Wex, H., Winkler, P. M., Carslaw, K. S., Worsnop, D. R., Baltensperger, U., and Kulmala, M.: Role of sulphuric acid, ammonia and galactic cosmic rays in atmospheric aerosol nucleation, Nature, 476, 429–U77, 2011.

Kuang, C., McMurry, P. H., McCormick, A. V., and Eisele, F. L.: Dependence of nucleation rates on sulfuric acid vapor concentration in diverse atmospheric locations, J. Geophys. Res.-Atmos.,113, 2008.

Kulmala, M., Hameri, K., Aalto, P. P., Makela, J. M., Pirjola, L., Nilsson, E. D., Buzorius, G., Rannik, U., Dal Maso, M., Seidl, W., Hoffman, T., Janson, R., Hansson, H. C., Viisanen, Y., Laaksonen, A., and O’Dowd, C. D.: Overview of the international project on biogenic aerosol formation in the boreal forest (BIO- FOR), Tellus Series B-Chemical and Physical Meteorology, 53, 324–343, 2001.

Kulmala, M.: How particles nucleate and grow, Science, 302, 1000–1001, 2003.

Kulmala, M., Lehtinen, K. E. J., and Laaksonen, A.: Cluster activation theory as an explanation of the linear dependence between formation rate of 3nm particles and sulphuric acid concentration, Atmos. Chem. Phys., 6, 787–793, 2006.

Kulmala, M., Kontkanen, J., Junninen, H., Lehtipalo, K., Manni- nen, H. E., Nieminen, T., Petaja, T., Sipila, M., Schobesberger, S., Rantala, P., Franchin, A., Jokinen, T., Jarvinen, E., Aijala, M., Kangasluoma, J., Hakala, J., Aalto, P. P., Paasonen, P., Mikkila, J., Vanhanen, J., Aalto, J., Hakola, H., Makkonen, U., Ruuska- nen, T., Mauldin, R. L., Duplissy, J., Vehkamaki, H., Back, J., Kortelainen, A., Riipinen, I., Kurten, T., Johnston, M. V., Smith, J. N., Ehn, M., Mentel, T. F., Lehtinen, K. E. J., Laaksonen, A., Kerminen, V. M., and Worsnop, D. R.: Direct Observations of Atmospheric Aerosol Nucleation, Science, 339, 943–946, 2013.

Laaksonen, A., Hamed, A., Joutsensaari, J., Hiltunen, L., Cavalli, F., Junkermann, W., Asmi, A., Fuzzi, S., and Facchini, M. C.: Cloud condensation nucleus production from nucleation events at a highly polluted region, Geophys. Res. Lett., 32, 4, 2005.

Levin, E. J. T., Prenni, A. J., Petters, M. D., Kreidenweis, S. M., Sullivan, R. C., Atwood, S. A., Ortega, J., DeMott, P. J., and Smith, J. N.: An annual cycle of size-resolved aerosol hygroscopicity at a forested site in Colorado, J. Geophys. Res.-Atmos., 117, 2012.

Levin, E. J. T., Prenni, A. J., Palm, B. B., Day, D. A., Campuzano-Jost, P., Winkler, P. M., Kreidenweis, S. M., DeMott, P. J., Jimenez, J. L., and Smith, J. N.: Size-resolved aerosol composition and its link to hygroscopicity at a forested site in Colorado, Atmos. Chem. Phys., 14, 2657–2667, 2014.

Lin, Yuh-Langand Farley, R. D. and Orville, H. D.: Bulk parameterization of the snow field in a cloud model, J. Climate Appl. Meteorol., 22, 1065–92, 1983.

Liu, X., Easter, R. C., Ghan, S. J., Zaveri, R., Rasch, P., Shi, X., Lamarque, J. F., Gettelman, A., Morrison, H., Vitt, F., Conley, A., Park, S., Neale, R., Hannay, C., Ekman, A. M. L., Hess, P., Mahowald, N., Collins, W., Iacono, M. J., Bretherton, C. S., Flanner, M. G., and Mitchell, D.: Toward a minimal representation of aerosols in climate models: description and evaluation in the Community Atmosphere Model CAM5, Geosci. Model Dev., 5, 709–739, 2012.

Luo, G. and Yu, F.: Simulation of particle formation and number concentration over the Eastern United States with the WRF- Chem plus APM model, Atmos. Chem. Phys., 11, 11521–11 533, 2011.

Matsui, H., Koike, M., Kondo, Y., Takegawa, N., Wiedensohler, A., Fast, J. D., and Zaveri, R. A.: Impact of new particle formation on the concentrations of aerosols and cloud condensation nuclei around Beijing, J. Geophys. Res.-Atmos., 116, 19, 2011.

McFiggans, G., Artaxo, P., Baltensperger, U., Coe, H., Facchini, M. C., Feingold, G., Fuzzi, S., Gysel, M., Laaksonen, A., Lohmann, U., Mentel, T. F., Murphy, D. M., O'Dowd, C. D., Snider, J. R., and Weingartner, E.: The effect of physical and chemical aerosol properties on warm cloud droplet activation, Atmos. Chem. Phys., 6, 2593–2649, 2006.

McMurry, P. H., Fink, M., Sakurai, H., Stolzenburg, M. R., Mauldin, R. L., Smith, J., Eisele, F., Moore, K., Sjostedt, S., Tanner, D., Huey, L. G., Nowak, J. B., Edgerton, E., and Voisin, D.: A criterion for new particle formation in the sulfur-rich Atlanta atmosphere, J. Geophys. Res.-

Atmos., 110, 10, 2005.

Merikanto, J., Spracklen, D. V., Mann, G. W., Pickering, S. J., and Carslaw, K. S.: Impact of nucleation on global CCN, Atmos. Chem. Phys., 9, 8601–8616, 2009.

Mikkonen, S., Romakkaniemi, S., Smith, J. N., Korhonen, H., Petaja, T., Plass-Duelmer, C., Boy, M., McMurry, P. H., Lehti- nen, K. E. J., Joutsensaari, J., Hamed, A., Mauldin, R. L., I., Bir- mili, W., Spindler, G., Arnold, F., Kulmala, M., and Laaksonen, A.: A statistical proxy for sulphuric acid concentration, Atmos. Chem. Phys., 11, 11 319–11 334, 2011.

Mlawer, E. J., Taubman, S. J., Brown, P. D., Iacono, M. J., and Clough, S. A.: Radiative transfer for inhomogeneous atmospheres: RRTM, a validated correlated-k model for the longwave, J. Geophys. Res.-Atmos., 102, 16 663–16 682, 1997.

O'Dowd, C. D., et al., A dedicated study of New Particle Formation and Fate in the Coastal Environment (PARFORCE): Overview of objectives and achievements, J. Geophys. Res., 107(D19), 8108, doi:10.1029/2001JD000555, 2002.

Ortega, J., Turnipseed, A., Guenther, A. B., Karl, T. G., Day, D. A., Gochis, D., Huffman, J. A., Prenni, A. J., Levin, E. J. T., Krei- denweis, S. M., DeMott, P. J., Tobo, Y., Patton, E. G., Hodzic, A., Cui, Y. Y., Harley, P. C., Hornbrook, R. S., Apel, E. C., Monson, R. K., Eller, A. S. D., Greenberg, J. P., Barth, M. C., Campuzano-Jost, P., Palm, B. B., Jimenez, J. L., Aiken, A. C., Dubey, M. K., Geron, C., Offenberg, J., Ryan, M. G., Fornwalt, P. J., Pryor, S. C., Keutsch, F. N., DiGangi, J. P., Chan, A. W. H., Goldstein, A. H., Wolfe, G. M., Kim, S., Kaser, L., Schnitzhofer, R., Hansel, A., Cantrell, C. A., Mauldin, R. L., and Smith, J. N.: Overview of the Manitou Experimental Forest Observatory: site description and selected science results from 2008–2013, Atmos. Chem. Phys., 14, 6345–6367, 2014.

Petaja, T., Mauldin, R. L., Kosciuch, E., McGrath, J., Nieminen, T., Paasonen, P., Boy, M., Adamov, A., Kotiaho, T., and Kulmala, M.: Sulfuric acid and OH concentrations in a boreal forest site, Atmos. Chem. Phys., 9, 7435–7448, 2009.

Petters, M. D. and Kreidenweis, S. M.: A single parameter representation of hygroscopic growth and cloud condensation nucleus activity, Atmos. Chem. Phys., 7, 1961–1971, 2007.

Pierce, J. R. and Adams, P. J.: Uncertainty in global CCN concentrations from uncertain aerosol nucleation and primary emission rates, Atmos. Chem. Phys., 9, 1339–1356, 2009.

Pierce, J. R., Riipinen, I., Kulmala, M., Ehn, M., Petaja, T., Junninen, H., Worsnop, D. R., and Donahue, N. M.: Quantification of the volatility of secondary organic compounds in ultrafine particles during nucleation events, Atmos. Chem. Phys., 11, 9019– 9036, 2011.

Pierce, J. R., Leaitch, W. R., Liggio, J., Westervelt, D. M., Wain- wright, C. D., Abbatt, J. P. D., Ahlm, L., Al-Basheer, W., Cz- iczo, D. J., Hayden, K. L., Lee, A. K. Y., Li, S. M., Russell, L. M., Sjostedt, S. J., Strawbridge, K. B., Travis, M., Vlasenko, A., Wentzell, J. J. B., Wiebe, H. A., Wong, J. P. S., and Mac- donald, A. M.: Nucleation and condensational growth to CCN sizes during a sustained pristine biogenic SOA event in a forested mountain valley, Atmos. Chem. Phys., 12, 3147–3163, 2012.

Reddington, C. L., Carslaw, K. S., Spracklen, D. V., Frontoso, M. G., Collins, L., Merikanto, J., Minikin, A., Hamburger, T., Coe, H., Kulmala, M., Aalto, P., Flentje, H., Plass-Duelmer, C., Birmili, W., Wiedensohler, A., Wehner, B., Tuch, T., Sonntag, A., O'Dowd, C. D., Jennings, S.

G., Dupuy, R., Baltensperger, U., Weingartner, E., Hansson, H. C., Tunved, P., Laj, P., Sellegri, K., Boulon, J., Putaud, J. P., Gruening, C., Swietlicki, E., Roldin, P., Henzing, J. S., Moerman, M., Mihalopoulos, N., Kouvarakis, G., Zdimal, V., Zikova, N., Marinoni, A., Bonasoni, P., and Duchi, R.: Primary versus secondary contributions to particle number concentrations in the European boundary layer, Atmos. Chem. Phys., 11, 12 007–12 036, 2011.

Rosenfeld, D., U. Lohmann, G. B. Raga, C. D. O'Dowd, M. Kulmala, S. Fuzzi, A. Reissell, and M. O. Andreae, Flood or drought: How do aerosols affect precipitation?, Science, 321, 1309 – 1313, 2008.

Sihto, S. L., Kulmala, M., Kerminen, V. M., Dal Maso, M., Petaja, T., Riipinen, I., Korhonen, H., Arnold, F., Janson, R., Boy, M., Laaksonen, A., and Lehtinen, K. E. J.: Atmospheric sulphuric acid and aerosol formation: implications from atmospheric measurements for nucleation and early growth mechanisms, Atmos. Chem. Phys., 6, 4079–4091, 2006.

Sipila, M., Berndt, T., Petaja, T., Brus, D., Vanhanen, J., Strat- mann, F., Patokoski, J., Mauldin, Roy L., I., Hyvarinen, A.-P., Lihavainen, H., and Kulmala, M.: The Role of Sulfuric Acid in Atmospheric Nucleation, Science, 327, 1243–1246, 2010.

Somers, C. M., McCarry, B. E., Malek, F., and Quinn, J. S.: Reduction of particulate air pollution lowers the risk of heritable mutations in mice, Science, 304, 1008–1010, 2004.

Spracklen, D. V., Carslaw, K. S., Kulmala, M., Kerminen, V. M., Mann, G. W., and Sihto, S. L.: The contribution of boundary layer nucleation events to total particle concentrations on regional and global scales, Atmos. Chem. Phys., 6, 5631–5648, 2006.

Stohl, A., Forster, C., Frank, A., Seibert, P., and Wotawa, G.: Tech- nical note: The Lagrangian particle dispersion model FLEX- PART version 6.2, Atmos. Chem. Phys., 5, 2461–2474, 2005.

Westervelt, D. M., Pierce, J. R., Riipinen, I., Trivitayanurak, W., Hamed, A., Kulmala, M., Laaksonen, A., Decesari, S., and Adams, P. J.: Formation and growth of nucleated particles into cloud condensation nuclei: model-measurement comparison, At- mos. Chem. Phys., 13, 7645–7663, 2013.

Wexler, A. S., Lurmann, F. W., and Seinfeld, J. H.: Modeling Urban and Regional Aerosols. I. Model Development, Atmos. Environ., 28, 531–546, 1994.

Young, L. H., Benson, D. R., Kameel, F. R., Pierce, J. R., Jun- ninen, H., Kulmala, M., and Lee, S. H.: Laboratory studies of H2SO4/H2O binary homogeneous nucleation from the SO2+OH reaction: evaluation of the experimental setup and preliminary results, Atmos. Chem. Phys., 8, 4997–5016, 2008.

Zaveri, R. A. and Peters, L. K.: A new lumped structure photochemical mechanism for large-scale applications, J. Geophys. Res.- Atmos., 104, 30 387–30 415, 1999.

Zaveri, R. A., Easter, R. C., Fast, J. D., and Peters, L. K.: Model for Simulating Aerosol Interactions and Chemistry (MOSAIC), J. Geophys. Res.-Atmos., 113, 29, 2008.

Zhang, H., Zhang, Z., Cui, T., Lin, Y.-H., Bhathela, N. A., Or- tega, J., Worton, D. R., Goldstein, A. H., Guenther, A., Jimenez, J. L., Gold, A., and Surratt, J. D.: Secondary Organic Aerosol Formation via 2-Methyl-3-buten-2-ol Photo oxidation: Evidence of Acid-Catalyzed Reactive Uptake of Epoxides, Environ. Sci. Technol., 1, 242–247, 2014.

Zhang, R. Y., Suh, I., Zhao, J., Zhang, D., Fortner, E. C., Tie, X. X., Molina, L. T., and Molina, M. J.: Atmospheric new particle formation enhanced by organic acids, Science, 304, 1487–1490, 2004.

Tables and Figures:

Table 1. Characteristics of four representative PBE days at the MEFO site during the BEACHON-RoMBAS-2011 field campaign. Metrics are reported for observations and the WRF-Chem model simulations (Nucleation-bsoa).

PBEs (<30nm) burst time (MST)		Growth rate[a]	J_{5nm}[b]	J_{50nm}	J_{130nm}	$N_{4\text{-}40nm}$[c]		$N_{40\text{-}100nm}$	
						max	mean	max	mean

07-28 10:20	Observation	2.5	0.74	0.21	0.01	20,540	16,155	4,160	3,795
	Model	3.0	1.09	0.20	0.02	34,440	31,515	5,389	5,357
07-29 12:25	Observation	2.0	N/A	0.24	0.02	31,710	27,865	13,410	11,622
	Model	3.7	N/A	0.11	0.03	10,650	9,551	5,342	5,282
08-10 10:20	Observation	2. 5	N/A	0.08	0.01	22,000	21,470	6,562	5,336
	Model	N/A	N/A	0.02	0.004	3,055	2,968	5,321	5,178
Average	Observation	2.3	0.74	0.18	0.013				
	Model	3.4	1.09	0.11	0.018				

a. Growth rate of ultrafine particles from 4 to 40 nm, in nm/hr.
b. J: Formation rate of small particles ~5nm, ~50nm and ~130nm, in $cm^{-3}s^{-1}$.
c. Number concentration of particles at 4-40nm and 40-100nm, in $\#/cm^3$. The mean values are averaged over a two-hour time period following the peak of each PBE. In the model, values from particles in 3.98 to 39.8nm , and from particles in 39.8 to 100nm are evaluated using observed $N_{4\text{-}40nm}$ and $N_{40\text{-}100nm}$.
Here, we report particles from 4 to 40 nm instead of 4 to 30 nm in order to have a closer match with the corresponding bins in the simulations.

Table 2. Description of model simulations: AN is activation nucleation parameterization, and BHN is binary homogeneous nucleation parameterization, which is the default option in the WRF-Chem model (see sections 1 and 3.2).

Simulations	Number of aerosol	Nucleation parameterizations	Accounting for condensation

	bins	Within PBL	Above PBL	of biogenic VOCs
Ref-8bins	8 bins (40nm-10μm)	BHN		No
Nucleation-on	20 bins (1nm-10μm)	AN	BHN	No
Nucleation-bsoa	20 bins (1nm-10μm)	AN	BHN	Yes
Nucleation-off	20 bins (1nm-10μm)	None		Yes

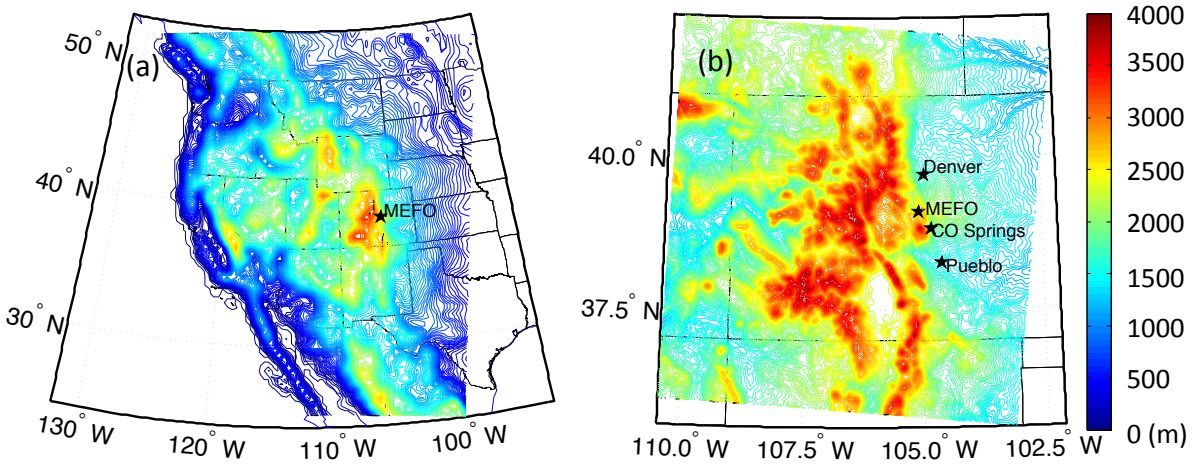

Figure 1: WRF-Chem domains. (a) Coarse domain covers the western US with 36 x 36 km^2 horizontal resolution, (b) Nested domain covers Colorado with 4 x 4km^2 resolution. Maps also show the topography, and the locations of the MEFO site, Denver, Colorado Springs, and Pueblo.

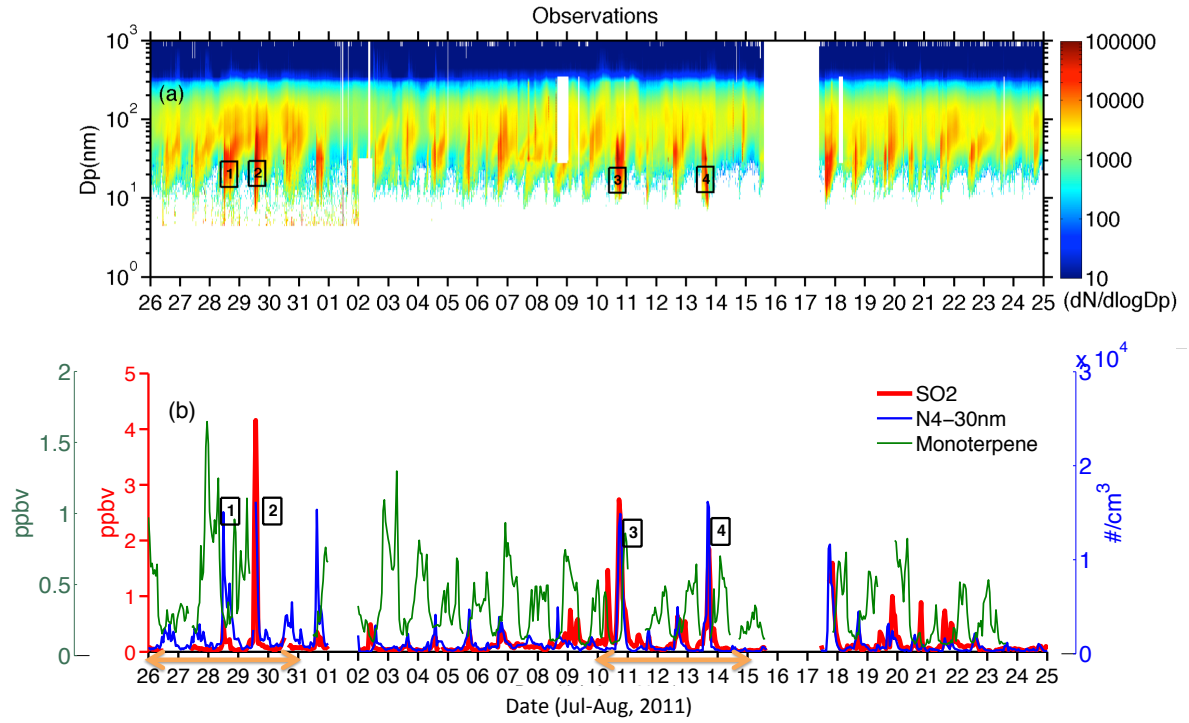

Figure 2: (a) Time series of number size distribution of submicron particles during BEACHON-RoMBAS. (b) Temporal variations in number concentrations of 4-30 nm diameter particles ($N_{4\text{-}30nm}$) (blue), SO_2 (red), and monoterpene (green) mixing ratios during the campaign. The four PBEs are selected (July 28 and 29, and August 10 and 13) for comparisons with the model. The orange lines indicate the periods simulated with WRF-Chem.

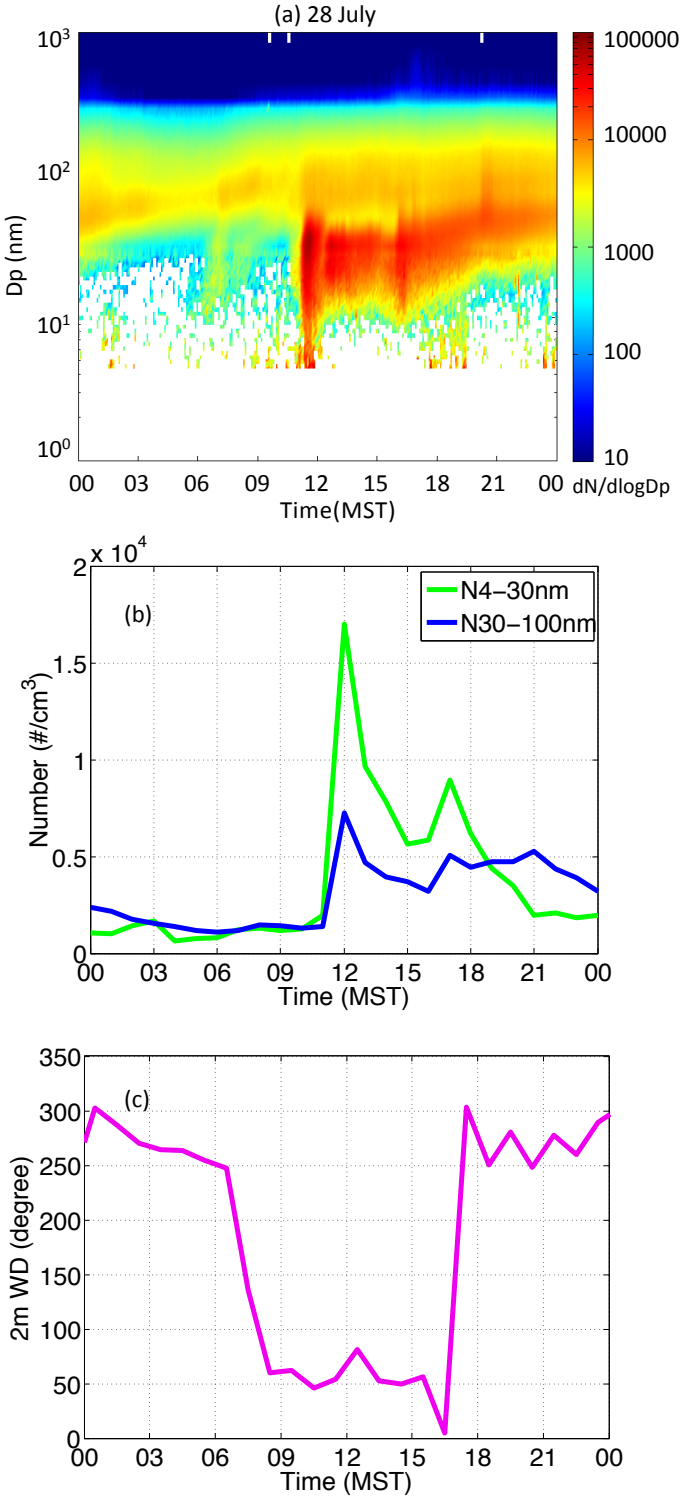

Figure 3: July 28: (a) shows the diurnal cycle of the number size distributions. (b) shows the diurnal cycle of number concentrations for particles from 4 to 30nm and 30 to 100nm. (c) shows the diurnal cycle of wind directions at 2 m.

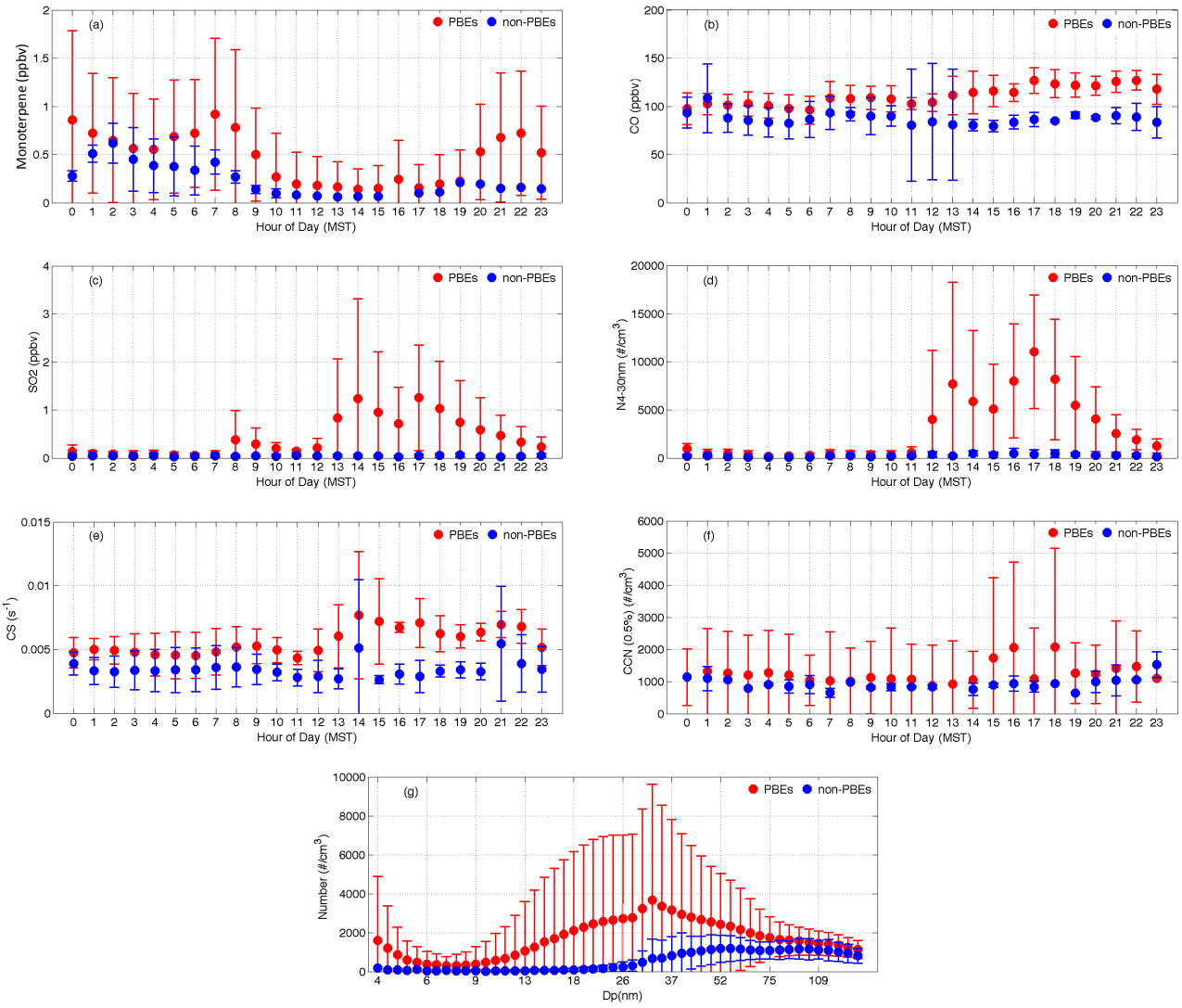

Figure 4: Comparison of measured parameters at the MEFO site during PBE and non-PBE days including hourly averaged diurnal profiles of (a) monoterpenes, (b) CO, (c) SO_2, (d) number concentrations of 4-30 nm diameter particles, (e) Condensation sinks (CS, s^{-1}), (f) CCN concentrations at 0.5% supersaturation, and (g) Number size distribution (from 4.4-150 nm). Error bars indicate 1σ variability.

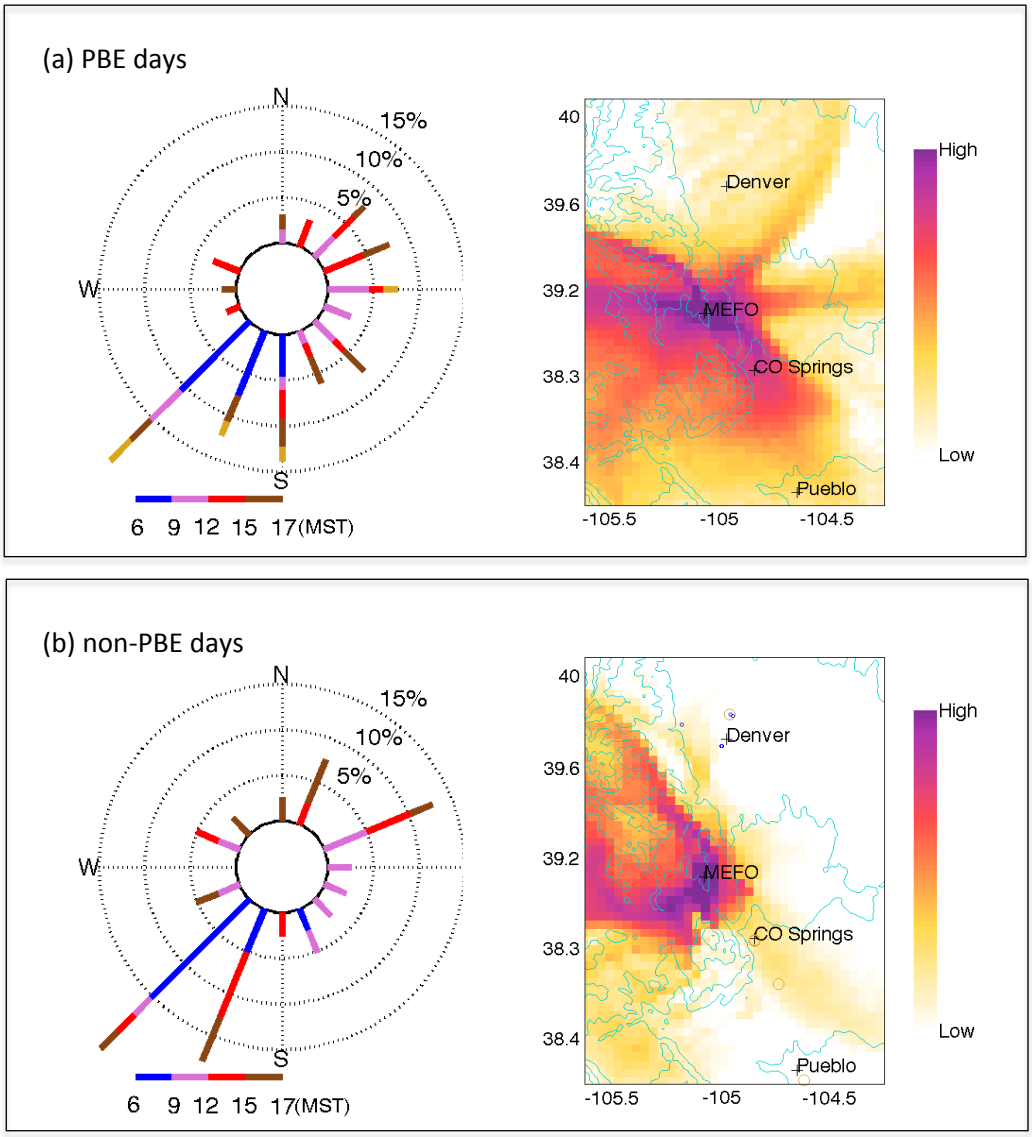

Figure 5: Wind fields for PBE days (a) and non-PBE days (b): Left panels are wind roses of local wind variations at 30 meters height plotted by hours of day at MEFO from 6:00 to 18:00 MS. Right panels are regional wind preferred directions corresponding to local wind roses respectively, based on WRF-FLEXPART analysis.

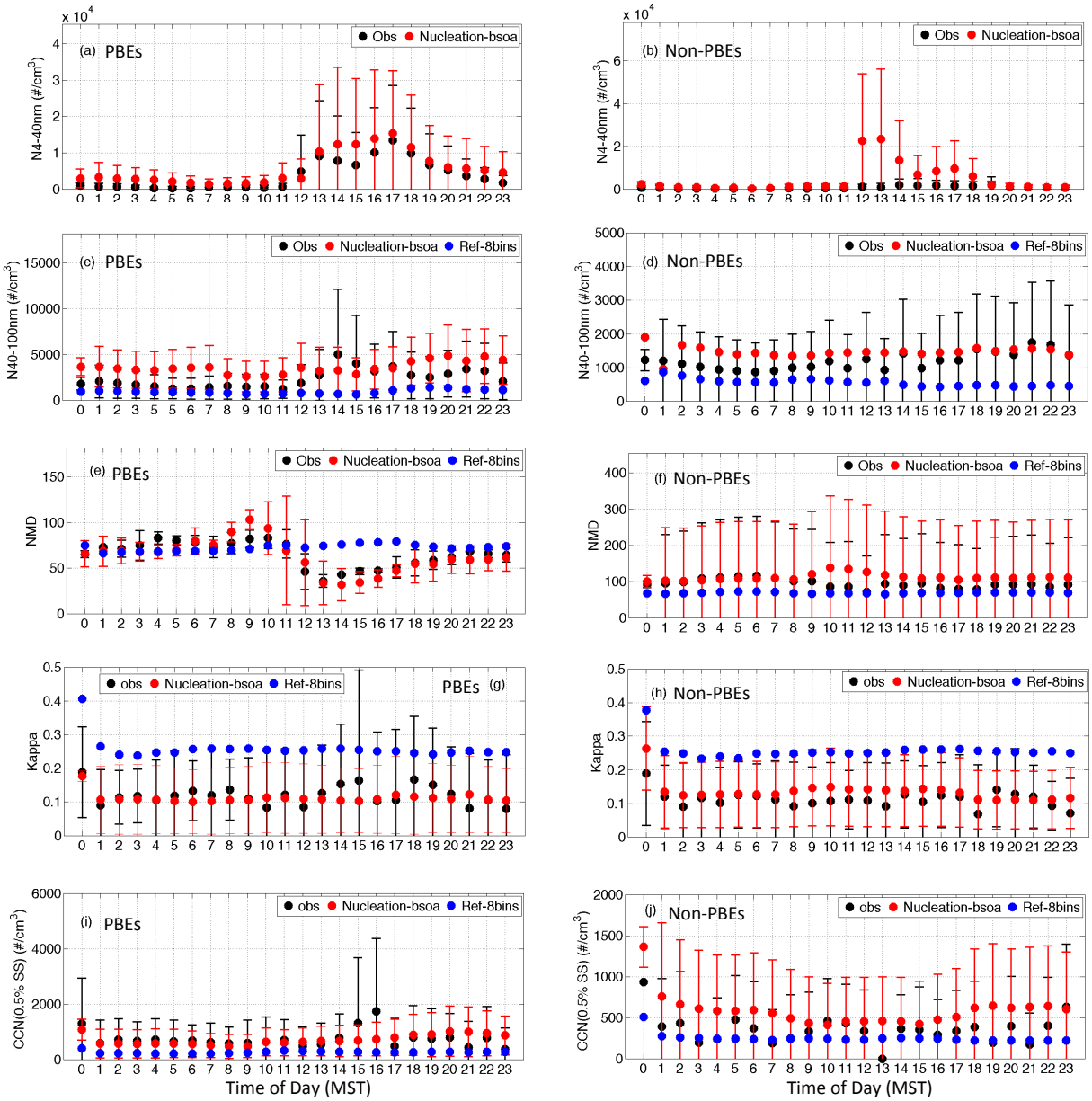

Figure 6: Comparison between measurements and simulations in diurnal profiles during PBE days (left column) and Non-PBE days (right column). Black dots are observations, red dots are simulations from Nucleation-bsoa run, and blue dots are simulations from Ref-8bins run. Error bars show 1σ variability. Plots show diurnal variations in (a,b) number concentrations of 4 to 40 nm particles ($N_{4\text{-}40nm}$) and (c,d) of 40 to 100 nm particles ($N_{40\text{-}100nm}$), diurnal profiles of (e,f) the number mean diameters (NMD), (g,h) Kappa values, and (i,j) number concentrations of CCN at 0.5% SS.

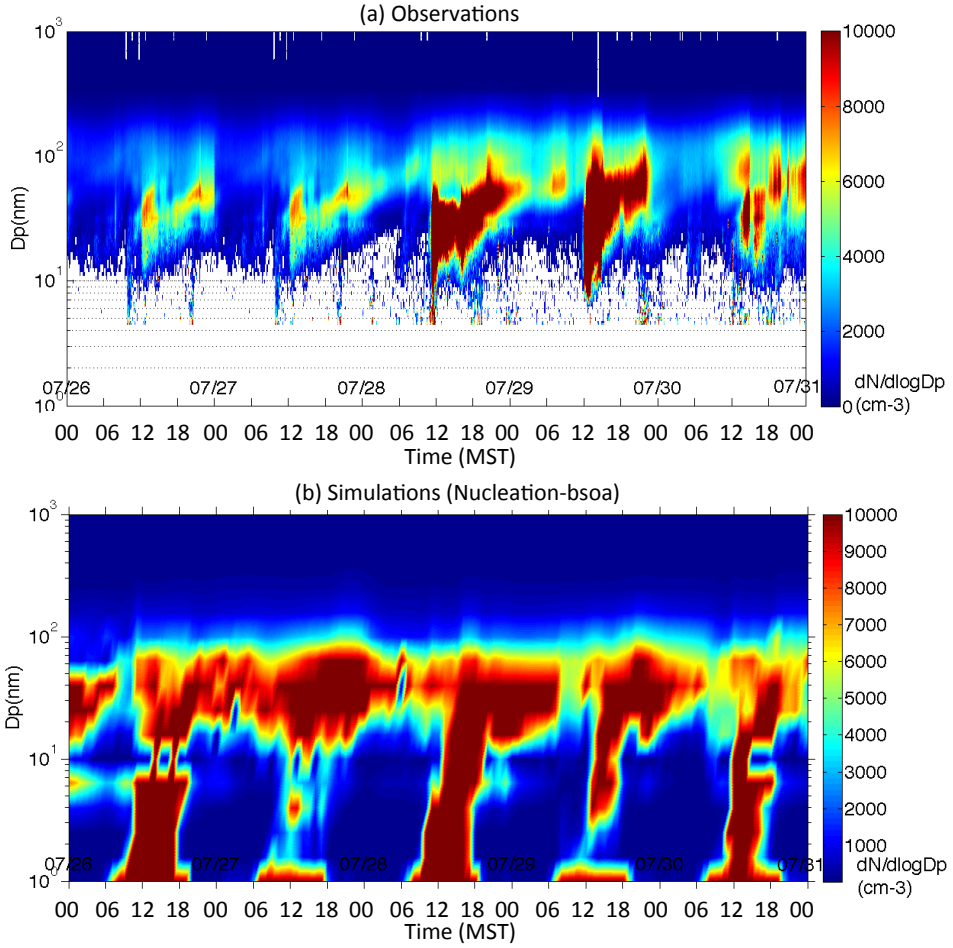
(a) Observations
Dp(nm)
10^3
10^2
10^1
10^0
07/26
07/27
07/28
07/29
07/30
07/31
00 06 12 18 00 06 12 18 00 06 12 18 00 06 12 18 00 06 12 18 00
Time (MST)
10000
8000
6000
4000
2000
0
dN/dlogDp
(cm-3)
(b) Simulations (Nucleation-bsoa)
Dp(nm)
10^3
10^2
10^1
10^0
07/26
07/27
07/28
07/29
07/30
07/31
00 06 12 18 00 06 12 18 00 06 12 18 00 06 12 18 00 06 12 18 00
Time (MST)
10000
9000
8000
7000
6000
5000
4000
3000
2000
1000
dN/dlogDp
(cm-3)

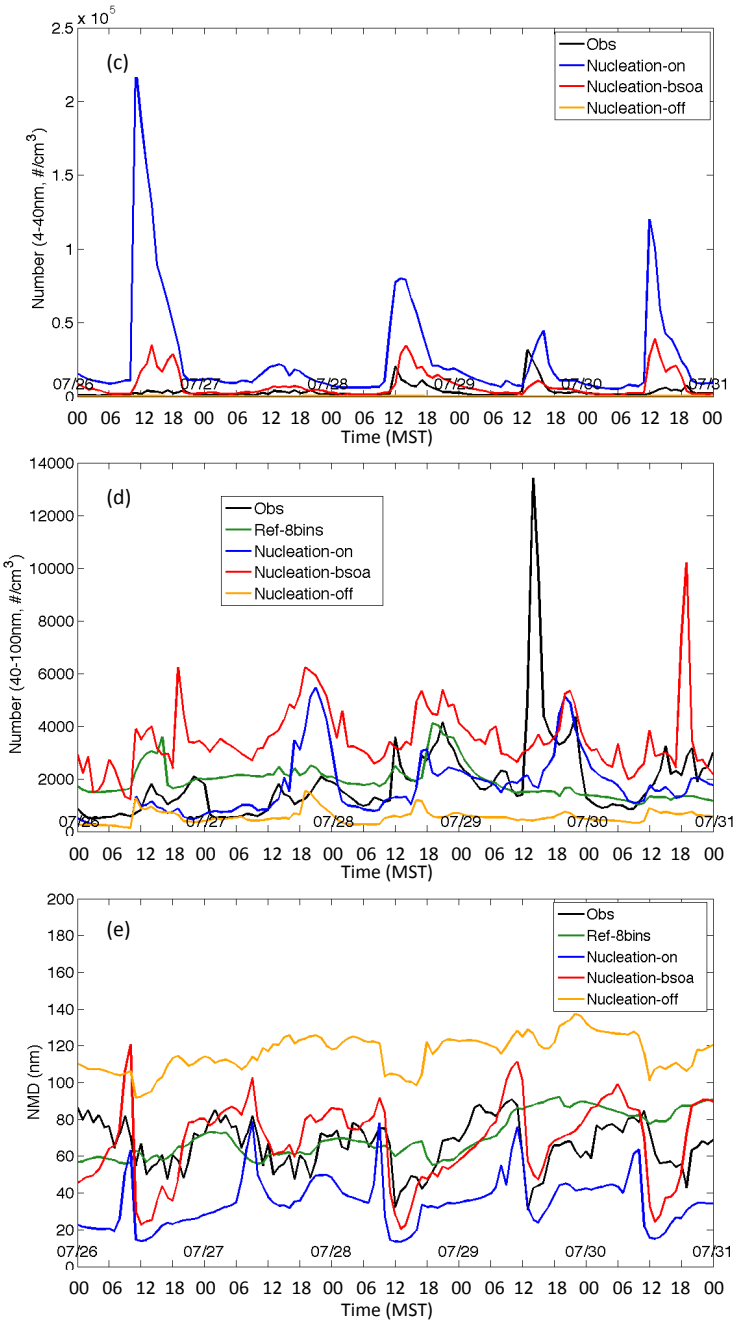

Figure 7: Temporal evolution of the (a) observed and (b) simulated (Nucleation-bsoa) number size distributions, during July 26-30, 2011. Time series of number concentrations of particles in size ranges of (c) 4-40nm and (d) 40-100nm, and (e) number mean diameter (NMD, see equation 1) as observed and predicted at the MEFO site. Measurements are indicated by the black line (OBS), base case is green, "Nucleation-on" is blue, "Nucleation-bsoa" is red, and "Nucleation-off" is orange, respectively (see Table 2 for the model run descriptions).

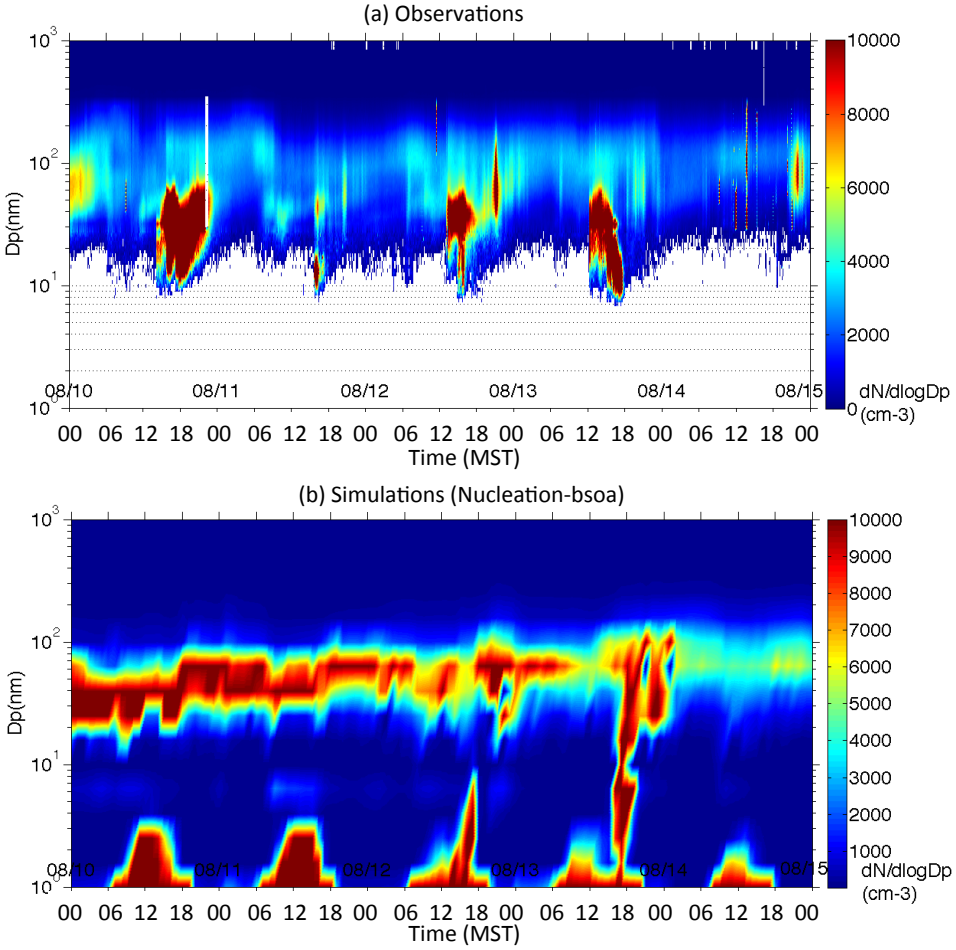
(a) Observations
Dp(nm)
10^3
10^2
10^1
10^0
08/10
08/11
08/12
08/13
08/14
08/15
00 06 12 18 00 06 12 18 00 06 12 18 00 06 12 18 00 06 12 18 00
Time (MST)
10000
8000
6000
4000
2000
0
dN/dlogDp
(cm-3)
(b) Simulations (Nucleation-bsoa)
Dp(nm)
10^3
10^2
10^1
10^0
08/10
08/11
08/12
08/13
08/14
08/15
00 06 12 18 00 06 12 18 00 06 12 18 00 06 12 18 00 06 12 18 00
Time (MST)
10000
9000
8000
7000
6000
5000
4000
3000
2000
1000
dN/dlogDp
(cm-3)

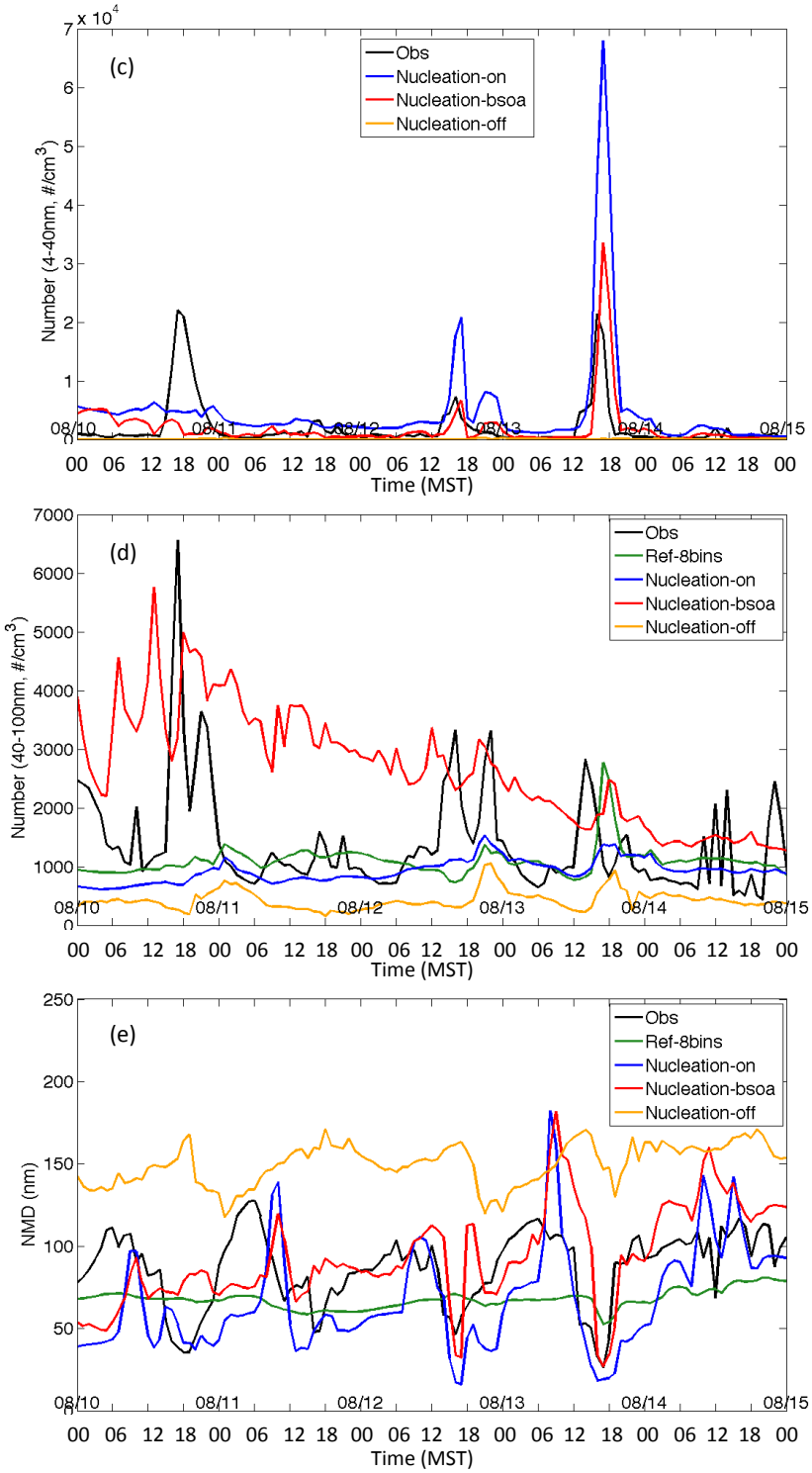

Figure 8: Similar to Figure 7 but for the August 10-14, 2011 time period.

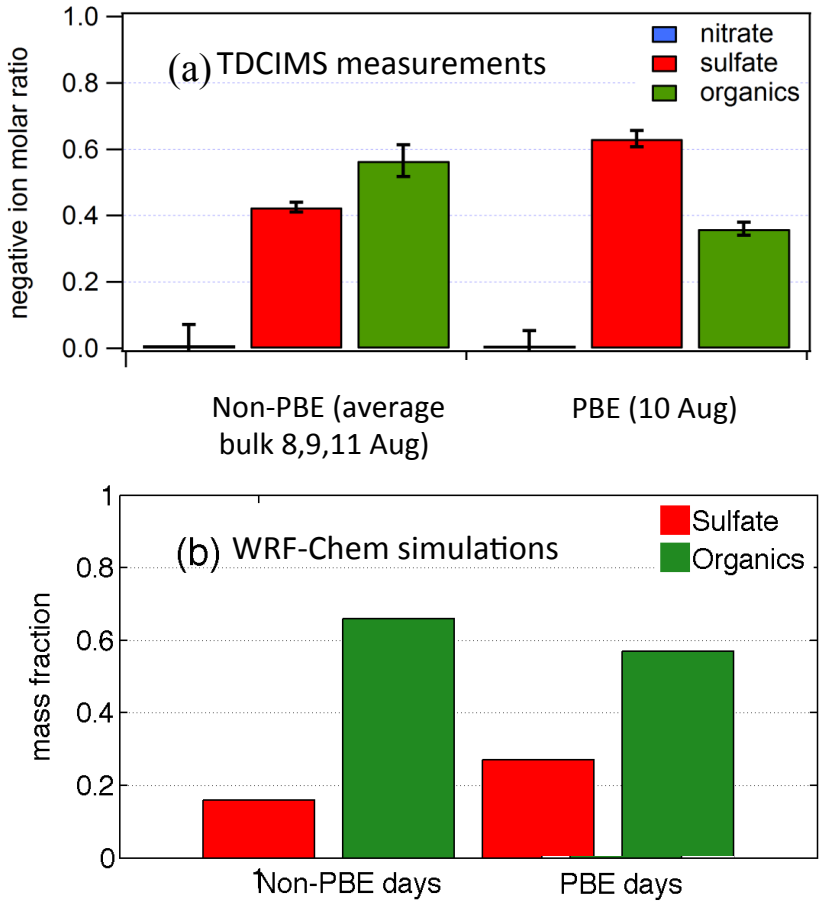

Figure 9: (a) TDCIMS measurements of negative ion molar ratios in bulk submicron aerosols during Non-PBE days (8, 9, 11 August) and in 20 nm (± ½ nm) particles during a PBE day (10 August). (b) Changes in simulated mass fractions of sulfate and organics in ~20nm particles between PBE days (Jul 28, 29, and August 10) and non-PBE days (August 11 and 14).

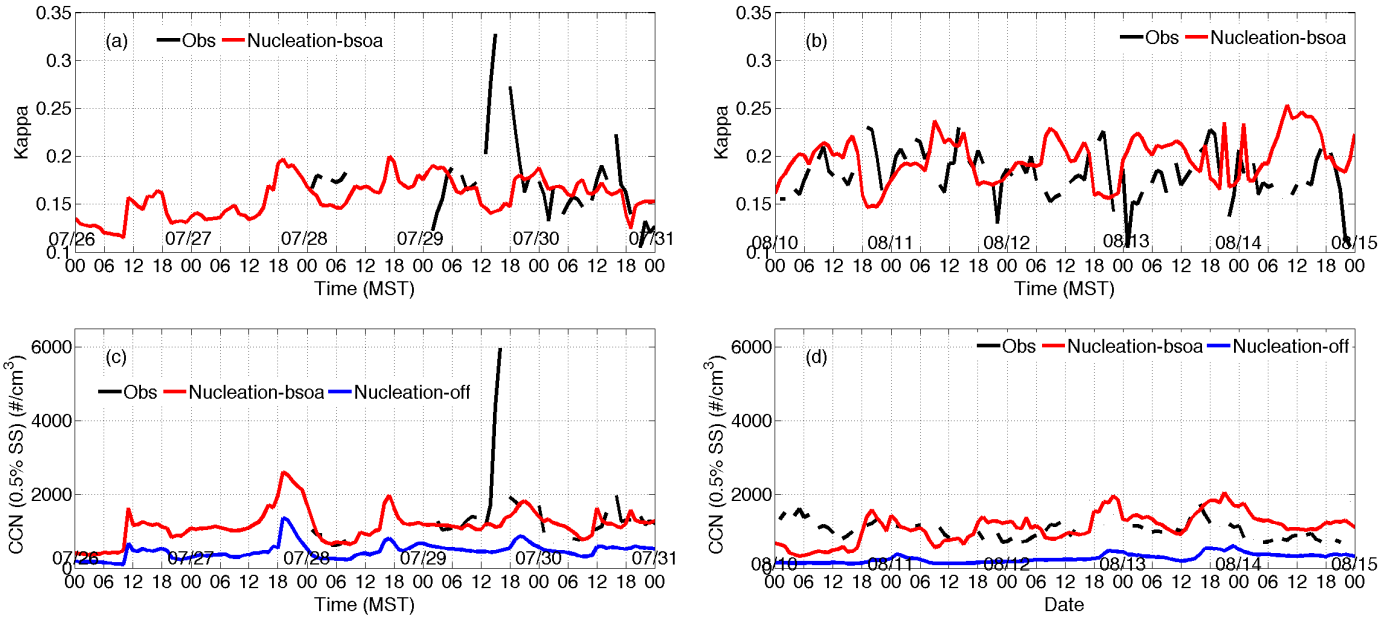

Figure 10: Observed and predicted (Nucleation-bsoa) (a,b) volume-averaged hygroscopicity (Kappa) and (c,d) CCN concentrations at high supersaturation condition (0.5% SS) from 26-30 July and 10-14 August 2011. The blue line shows the results without nucleation within PBL from "Nucleation-off" model run.